Effectiveness of emission control to reduce $PM_{2.5}$ pollution of Central China during winter haze episodes under various potential synoptic controls

Yingying Yan [1#], Yue Zhou [2#], Shaofei Kong [1, 4*], Jintai Lin [3], Jian Wu [1, 4], Huang Zheng [1, 4], Zexuan Zhang [1, 4], Aili Song [1], Yongqing Bai [2], Zhang Ling [2], Dantong Liu [5], Tianliang Zhao [6]

[1] Department of Atmospheric Sciences, School of Environmental Studies, China University of Geosciences, Wuhan, 430074, China

[2] Hubei Key Laboratory for Heavy Rain Monitoring and Warning Research, Institute of Heavy Rain, China Meteorological Administration, Wuhan 430205, China

[3] Laboratory for Climate and Ocean-Atmosphere Studies, Department of Atmospheric and Oceanic Sciences, School of Physics, Peking University, Beijing 100871, China

[4] Department of Environmental Science and Engineering, School of Environmental Studies, China University of Geosciences, Wuhan, 430074, China

[5] Department of Atmospheric Sciences, School of Earth Sciences, Zhejiang University, Hangzhou, Zhejiang, China

[6] School of Atmospheric Physics, Nanjing University of Information Science and Technology, Nanjing, 210044, China

Correspondence to: Shaofei Kong (kongshaofei@cug.edu.cn)

[#] Contributed equally to this work

Abstract

Currently mitigating the severe particle pollution in autumn and winter is the key to further improve the air quality of China. The source contributions and transboundary transport of fine particles ($PM_{2.5}$) in pollution episodes are closely related to large-scale or synoptic-scale atmospheric circulation. Under different synoptic conditions, how to effectively reduce emissions to control haze pollution is rarely reported. In this study, we classify the synoptic conditions over Central China from 2013 to 2018 by using

Lamb-Jenkension method and the NCEP/NCAR FNL operational global analysis data. The effectiveness of emission control to reduce $PM_{2.5}$ pollution during winter haze episodes under potential synoptic controls is simulated by GEOS-Chem model. Among the ten identified synoptic patterns, four types account for 87% of the total pollution days. Two typical synoptic modes of them are characterized by small surface wind speed and stable weather conditions/high relative humidity (A/C-type) over Central China due to a high-pressure system/a southwest trough low-pressure system, blocking pollutants dispersion. Sensitivity simulations show that these two heavy pollution processes are mainly contributed by local emission sources with ~82% for A-type and ~85% for C-type, respectively. The other two patterns lead to pollution of transport characteristics affected by northerly/southerly winds (NW/SW-type), carrying air pollution from northern/southern China to Central China. The contribution of pollution transmission from North/South China is 36.9%/7.6% of $PM_{2.5}$ and local emission sources contribute 41%/69%. We also estimate the effectiveness of emission reduction in these four typical severe pollution synoptic processes. By only reducing SO_2 and NO_x emission and not controlling NH_3, the enhanced nitrate counteracts the effect of sulfate reduction on $PM_{2.5}$ mitigations, with less than 4% decrease in $PM_{2.5}$. In addition, to effectively mitigate haze pollution of NW/SW-type synoptic controlled episodes, local emission control actions should be in coordination with regional collaborative actions.

1 Introduction

The regional pollution of fine particles ($PM_{2.5}$) has attracted worldwide attention in the public and in the scientific community (Cheng et al., 2016; Li et al., 2017c; Lin et al., 2018; Bi et al., 2019) due to its detrimental effect on visibility (Wang et al., 2020) and public health (Agarwal et al., 2017; Zhang et al., 2017). The $PM_{2.5}$ pollution in China has been continuously alleviating since 2013 as the implication of the Air Pollution Prevention and Control Action Plan (Zheng et al., 2018; Zhang et al., 2019),

especially in the Beijing-Tianjin-Hebei region (BTH) (Li et al., 2017b; Cheng et al., 2019), the Yangtze River Delta (YRD) region and the Pearl River Delta (PRD) region. However, severe particle pollution still occurs frequently in autumn and winter, which is the major reason restricting the $PM_{2.5}$ to come up to national standard. For example, 12 extremely severe and persistent $PM_{2.5}$ pollution episodes occurred in Beijing in January 2013, February 2014, December 2015, December 2016 and January 2017 (Zhong et al., 2018; Sun et al., 2016; Wang et al., 2018). Currently, how to effectively reduce emissions in autumn and winter is the key to mitigate haze pollution in China.

The contribution of emission sources has been widely recognized as the decisive factor of $PM_{2.5}$ pollution over urban agglomerations, including industrial exhaust, urban transportation, residential emission, power plants, agricultural activities, and bio-combustion (Huang et al., 2014; Tian et al., 2016; Wu et al., 2018; An et al., 2019). While the outbreak, persistence and dissipation of particle pollution generally depends on the meteorological conditions and regional synoptic patterns, controlled by the large-scale or synoptic-scale atmospheric circulation (Chuang et al., 2008; Zhang et al., 2012; Russo et al., 2014; Zheng et al., 2015; Shu et al., 2017; Li et al., 2019).

Many studies have tried to reveal the relationship between synoptic patterns and severe particle pollution, and estimate the meteorological contributions to these pollution episodes. The YRD is mainly affected by pollutants transmitted from the northern and the southern China when the East Asian major trough is located at its front (Liao et al., 2017; Shu et al., 2017; Li et al., 2019). Liao et al. (2020) has confirmed that the relative position of the PRD to high-pressure systems imposes significant impacts on the diffusion conditions and the $PM_{2.5}$ distributions in the PRD region. For North China Plain (NCP), high frequency of stagnant weather accompanied by small pressure gradient and near-surface wind speed, and shallow mixing layer are major reasons of aerosol pollution over this region in winter (He et al., 2018). The aerosol pollution formation process in Sichuan Basin is often controlled by the large scale high-pressure circulation at sea level (Sun et al., 2020). In the Guanzhong basin, pollution event is

generally governed by both the large-scale synoptic situation and the small-scale local circulation. The downhill wind not only forms a convergence zone in the basin, but also makes pollutants flow back from the mountain region to the basin (Bei et al., 2017). Leung et al. (2018) also find strong correlations of daily $PM_{2.5}$ variability with several synoptic patterns, including monsoon flows and cold front channels in northern China related to the Siberian High, onshore flows in eastern China, and frontal rainstorms in southern China. These previous studies have highlighted that different levels of $PM_{2.5}$ pollutions are closely related to the dominant synoptic patterns in different regions, and they attribute the large spatial variability of pollution to the regional transport contributions, not only the different local sources of $PM_{2.5}$. Thus, heavy pollution prevention and control needs to consider the weather situation, otherwise local emission reduction measures would not work well. However, under different synoptic conditions, how to effectively reduce local and regional emissions to control haze pollution is rarely reported.

Various key regions have issued the emergency preplan against the winter haze episodes, while these schemes can only be targeted at a certain city (The People's Government of Beijing Municipality, 2018; The People's Government of Shanghai Municipality, 2018) or a certain urban agglomeration (The People's Government of Guangdong Province, 2014). Although there are many studies targeted $PM_{2.5}$ mitigations at a regional scale (Ding et al., 2019; Zhang et al., 2019, Xing et al., 2018, 2019; Fu et al., 2017; etc.), their results can not be directly applied to reduce winter $PM_{2.5}$ pollution under various synoptic controls. Moreover, current emission reduction policies in China mainly aimed at sulfur dioxide (SO_2) and nitrogen dioxide (NO_2), ignoring the effective emission reduction on ammonia (NH_3), although some modeling works have discussed the effectiveness of ammonia emission reduction for $PM_{2.5}$ mitigations (Liu et al., 2019; Ye et al., 2019; Xu et al., 2019; Bai et al., 2019). Compared to remarkable reduction in SO_2, NO_2, and primary PM emissions, NH_3 emissions has remained stable during 2014–2018 in China (Zheng et al., 2018). In addition, given the

114 important roles of other $PM_{2.5}$ precursors (eg., NMVOCs) in aerosol formation (Geng
115 et al., 2019), cutting non-SO_2-NO_2-PM emissions should be proposed as a next-step
116 mitigation strategy. Therefore, for $PM_{2.5}$ mitigations in a specific region during winter
117 haze episodes forced by various synoptic conditions, whether the air pollution
118 emergency management and control schemes are effective and how to improve them
119 have become an urgent scientific question to be answered.

120 In order to investigate the effectiveness of emission control to reduce $PM_{2.5}$
121 pollution during winter haze episodes under various potential synoptic controls (PSCs),
122 we take the severe particle pollution of winter haze episodes over Jingzhou, the
123 hinterland of Yangtze River middle basin in Central China, as an example. Central
124 China is geographically surrounded by major haze pollution regions, the SCB to the
125 west, the PRD to the south, the YRD to the east, and the NCP to the north (Fig. 1). As
126 a regional pollutant transport hub with sub basin topography, Central China is a region
127 of transmission-pollution characteristics affected by two reported transport pathways
128 from the vast flatland in central eastern China (Yu et al., 2020) and from the NCP region
129 (Zheng et al., 2019a). In combination with high anthropogenic emissions (Wu et al.,
130 2018) and secondary aerosol formation (Huang et al., 2020), Central China often suffers
131 severe pollution episodes in winter caused by $PM_{2.5}$ (Gong et al., 2015; Xu et al., 2017).
132 In this study, we conduct the circulation classification to differentiate the synoptic
133 modes during the severe particle pollution episodes in winter over Central China from
134 2013 to 2018 by using Lamb-Jenkension method. Then we simulate the $PM_{2.5}$ chemical
135 components, and the contributions of local sources as well as transboundary transport
136 of $PM_{2.5}$ under different synoptic conditions. Finally, the effectiveness of emission
137 reduction in main potential synoptic patterns are evaluated by GEOS-Chem model
138 simulations. This study combines the atmospheric (circulation classification) and
139 environmental (chemical transport modeling) research methods and could provide
140 reference for emission control of severe winter haze pollution under different weather
141 types, and provide basis for regional air quality policy-making.

2 Data and Methods

2.1 Data

Hourly mass concentrations of $PM_{2.5}$ at Jingzhou (112.18°E, 30.33°N, 33.7 m) from November 2013 to December 2018 are obtained from Hubei Environmental Monitoring Central Station (http://sthjt.hubei.gov.cn/). We screen the pollution days with daily mean $PM_{2.5}$ concentrations larger than 150 $\mu g/m^3$ for circulation classification.

Figure 1

We use the daily mean sea level pressure (SLP) between 2013 and 2018 from the National Centers for Environmental Prediction/National Center for Atmospheric Research (NCEP/NCAR) Final (FNL) Operational Global Analysis data (horizontal resolution: 1° × 1°; temporal resolution: 6 hours; https://rda.ucar.edu/datasets/ds083.3/) to conduct the classification of Lamb-Jenkension circulation types.

The meteorological data of surface observations at Jingzhou, including ambient temperature, relative humidity, wind speed, wind direction and atmospheric pressure, are obtained from Hubei Meteorological Information and Technology Support Center (http://hb.cma.gov.cn/qxfw/index.html). The data from November 2013 to February 2014 are used to analyze the meteorological characteristics during the period four severe particle pollution events occurred in succession over Central China (Fig. S1).

In order to better evaluate the GEOS-Chem model performances, we also use the $PM_{2.5}$ observations (a total of 633 sites; from November 2013 to February 2014) from Ministry of Ecology and Environment of China (MEE, http://www.mee.gov.cn/) to conduct the model-observation comparison.

2.2 Lamb-Jenkension Circulation Classification

The atmospheric circulation classification adopts the Lamb-Jenkension method proposed by Lamb et al. (1950) and developed by Jenkension et al. (1977). Compared to the objective classification method PCA used in some studies (Chang and Zhan, 2017, Dai et al., 2021), this Lamb-Jenkension method is a combination of subjective and objective methods. After the objective judgment of the circulation, we also make subjective considerations to overcome the weaknesses of their respective, leading to better synoptic significance. Many works of circulation classification have used the Lamb-Jenkension method and reported that the analysis can well respond to the classification results (Philipp et al., 2016;Santurtun et al., 2015;Pope et al., 2015;Russo et al., 2014;Pope et al., 2014;Trigo and DaCamara, 2000).

To calculate the circulation types of Jingzhou, we mark total 16 points (97.5°E-127.5°E, 20°N-40°N) by every 10 longitudes and 5 latitudes and the center point located at 112.5° E and 30° N (Fig. S2). Using the sea level pressure of 16 points, we calculate six circulation indexes by scheme of central difference:

$$u = 0.5[P(12) + P(13) - P(4) - P(5)] \quad (1)$$

$$v = \frac{1}{\cos a} \times \frac{1}{4}[P(4) + 2P(9) + P(13) - P(4) - 2P(8) - P(12)] \quad (2)$$

$$\mathrm{V} = \sqrt{u^2 + v^2} \quad (3)$$

$$\xi_u = \frac{\sin\alpha}{2\sin\alpha_1}[P(15) + P(16) - P(8) - P(9)] - \frac{\sin\alpha}{2\sin\alpha_2}[P(8) + P(9) - P(1) - P(2)] \quad (4)$$

$$\xi_v = \frac{1}{8\cos^2\alpha}[P(6) + 2P(10) + P(14) - P(5) - 2P(9) - P(13) + P(3) + 2P(7) + P(11) - P(4) - 2P(8) - P(12)] \quad (5)$$

$$\xi = \xi_u + \xi_v \quad (6)$$

Where $P(n)(n = 1, 2, 3 \cdots 16)$ is the sea level pressure at the n^{th} point; α, α_1 and α_2 are the latitude values of points C, A_1 and A_2, respectively; V is the geostrophic wind, u and v are the latitudinal and meridional components of the geostrophic wind; ξ is the geostrophic vorticity; ξ_u is the u meridional gradient, and ξ_v is the v latitudinal gradient.

Taking the latitude of the center point as the reference frame, the unit of six circulation indexes is $hPa/(10^o lon)$, the direction of geostrophic wind can be determined by u and v, and cyclones and anticyclones can be determined by ξ. According to the geostrophic wind speed, wind direction and vorticity value, the circulation is divided into 10 types. The classification standard and corresponding types are shown in Table 1.

Table 1

2.3 GEOS-Chem simulations

The GEOS-Chem chemistry transport model is used (http://acmg.seas.harvard.edu/geos/) to simulate the spatiotemporal distribution of $PM_{2.5}$. The nested model, covering China (70°E-140°E, 15°S-55°N), is run with a horizontal resolution of 0.25° latitude × 0.3125° longitude and 72 vertical layers. The boundary condition of nested model is provided by the GEOS-Chem global model with a horizontal resolution of 2° latitude × 2.5° longitude (Fig. S3). Both global and nested simulations, driven by the GEOS-FP assimilated meteorological data, include detailed tropospheric Ozone-NO_x-VOCs-HO_x-aerosol chemistry. More details are shown in Yan et al. (2019). In the models, anthropogenic and natural sources are fully considered

in GEOS-Chem. Table S1 and Table S2 show a list of emission inventories in the global model and nested simulation, respectively. In China, the monthly grid data of 0.25° × 0.25° from MEIC inventory (http://meicmodel.org) for CO, NO_x, SO_2 and non-methane volatile organic compounds (NMVOCs) in 2013-2014 is used. Over Central China, anthropogenic sources of these species are from our group SEEA (Source Emission and Environment Research) inventory with the grid data of 0.1° × 0.1° (not shown). The SEEA emission inventory was developed based on the year of 2017 for the Wuhan city cluster and it has been successfully adopted for the air quality simulating and forecasting of 7th CISM Military World Games in 2019. Other emission descriptions are shown in Supplementary Sect. S1.

In order to better simulate the spatiotemporal distribution of $PM_{2.5}$ over Central China, especially in winter heavy pollution periods, the standard v11-01 of GEOS-Chem is optimized according to the actual situation in China (see details in Supplementary Sect. S2), including optimizing $PM_{2.5}$ sources and increasing the proportion of sulfate primary emission (Yan et al., 2020). The $PM_{2.5}$ primary anthropogenic emissions enhance the $PM_{2.5}$ concentrations over Central China by 5-20 $\mu g/m^3$ in winter (Fig. S4). Compared with the results before the model optimization (Fig. S5), the sulfate concentration simulated by the optimized model increased from 10-20 $\mu g/m^3$ to 30-50 $\mu g/m^3$. Further comparisons of $PM_{2.5}$ with observations and inorganic salts (sulfate, nitrate and ammonium) with reported values from previous studies are shown in Sect.3.3.

3. Results and Discussion

3.1 Classification of PSCs

As shown in Fig. 2, among the circulation patterns of pollution-day at Jingzhou from 2013 to 2018, the frequency of SW-type circulation is the highest, accounting for 29% of the total pollution days. The frequencies of NW-type, A-type and C-type are also high, accounting for 27%, 19% and 12%, respectively. While the other six

248 circulation patterns are less occurred, with the frequencies less than 5%. Thus, the
249 above four typical circulation types are considered as the main potential synoptic
250 controls of the severe particle pollution episodes over Central China.
251
252 Figure 2
253
254 **3.2 Characteristics of the four main PSCs**
255 SW-type circulation is the predominant PSC of severe $PM_{2.5}$ pollution episodes.
256 The circulation at 500 hPa is relatively flat and the whole East Asia region is affected
257 by the westerly flow (Fig. S6a). Westerly belt fluctuates greatly at 700 hPa and there
258 are two ridges and a southwest trough in the middle latitudes of Asia (Fig. S7a).
259 Jingzhou is located in the front of a trough, prevailing the weak southwest airflow. At
260 850 hPa, the cold high pressure center is formed in Xinjiang of China. Warm low
261 pressure appears in the low latitude area and weak high pressure appears in the East
262 China Sea (Fig. 3a). In combination with the surface field, a high-low-high saddle like
263 field forms from west to east (Fig. 4a). Such synoptic type is also the dominant weather
264 system of eastern China (Shu et al., 2017; Yang et al., 2018). Jingzhou is located in the
265 back of Bohai-northeast high pressure and the front of southwest warm low pressure.
266 Thus it is affected by the southerly airflow, which could be conducive to the transport
267 of air pollutants formed over southern China to Central China. Associated with small
268 local surface wind speed (< 3 m/s) at Jingzhou, the dispersion of local and transported
269 pollutants is inhibited.
270
271 Figure 3
272
273 NW-type circulation mainly occurs in the early winter (December and January).
274 This synoptic pattern is also reported as one of the main types to affect the aerosol
275 distributions over eastern China (Zheng et al., 2015). Circulation at 500 hPa is

276 controlled by one trough and one ridge, with the weak ridge located in the northwest of
277 China and the shallow trough located in the northeast of China (Fig. S6b). The whole
278 East Asia is affected by the westerly current. The trough and ridge at 700 hPa are
279 deepened. Jingzhou is located at the bottom of the shallow trough, prevailing the west-
280 northwest airflow, affected by the flow around the plateau (Fig. S7b). At 850 hPa, the
281 cold high pressure center is formed in Xinjiang, and Jingzhou is affected by the
282 northerly airflow, due to being in the front of the high pressure (Fig. 3b). For the sea
283 level pressure, the cold high pressure is located in the west of Mongolia and Xinjiang
284 of China (Fig. 4b). Jingzhou is located at the region with weak fluctuation in the front
285 of the high pressure, and the surface wind speed is smaller than 2 m/s. The haze episodes
286 induced by NW-type synoptic pattern is similar to the transmission-accumulation
287 pollution caused by SW-type, but the transmission path is from Northern China to
288 Central China.
289
290 Figure 4
291
292 A-type circulation also mainly occurs in the early winter. The high-altitude
293 circulation field is controlled by one trough and one ridge (Fig. S6c and S7c). East Asia
294 is affected by west-northwest air flow, and the SLP is controlled by a huge high
295 pressure, with the center located in the southwest of Baikal Lake (Fig. 4c). A surface
296 high pressure favors accumulation of air pollutants, especially over the regions of high
297 pressure center (Leung et al., 2018). Jingzhou is in the sparse pressure field in front of
298 the high pressure (Fig. 3c and 4c), with an average surface wind speed of ~1.3 m/s. The
299 uniform west-northwest air flow at high altitude would lead to the low water vapor
300 content and less cloud amount, which is conducive to radiation cooling at night. In
301 addition, due to the weak high pressure ridge in the north, it is not conducive to the
302 eastward and southward movement of cold air, leading to the stable weather situation

and thus severe haze pollution at Jingzhou. This type is also responsible for most of the severe particulate pollution days in the BTH and YRD regions (Li et al., 2019).

C-type circulation mainly occurs in late winter and early spring, when the relative humidity is large with an average value of 74%. East Asia is controlled by the straight westerly flow, and the southwest shallow trough is obvious at 500 hPa (Fig. S6d). Additionally, the West Pacific subtropical high extends to the west, Central China is affected by the southwest flow. Southwest trough is deepened at 700 hPa, and Jingzhou is located in front of the trough and controlled by the southwest airflow (Fig. S7d). High pressure at the south of Xinjiang and the north of Plateau is strengthened at 850 hPa, and the southwest low pressure center is formed (Fig. 3d). Jingzhou is located in the low pressure system on the SLP field (Fig. 4d), with small surface wind speed (0-3 m/s). Together with the large relative humidity, which can promote the hygroscopic growth of particulate matter (Twohy et al., 2009; Zheng et al., 2015), the haze pollution is persistent and serious at Jingzhou. The impact of low-pressure systems on winter heavy air pollution have also been reported in the northwest Sichuan Basin (Ning et al., 2018).

3.3 $PM_{2.5}$ and chemical components under the four main PSCs in control simulations

The spatiotemporal distribution of $PM_{2.5}$ and its components under the four typical synoptic controls over Central China were simulated by optimized GEOS-Chem model. In order to reduce the simulation cost, the continuous four severe haze episodes occurred during November, 2013-February, 2014 are selected. These four haze episodes are controlled by the synoptic pattern of SW-type (18-25 November, 2013), NW-type (19-26 December, 2013), A-type (14-21 January, 2014) and C-type (26 January - 2 February, 2014), respectively. The air quality at Jingzhou during the four pollution episodes is between grade 5 ($PM_{2.5}$ > 150 μg/m^3) and grade 6 heavy pollution ($PM_{2.5}$ > 250 μg/m^3, as Fig. 5a and S1a shown). The simulation time is started at

November 1st, 2013, with the first two weeks used as spin up to eliminate the impact of initial conditions.

Figure 5

Figure 6

The daily/hourly mean $PM_{2.5}$ concentrations at Jingzhou in the four typical heavy pollution processes simulated by the control (CON) simulation (Table 2) are compared with the observations (Fig. 5a/Fig. S1a). The model underestimates the observed $PM_{2.5}$ concentrations (by 43.3 μg/m^3 on average), especially in the high $PM_{2.5}$ periods (by 116.8 μg/m^3 at the maximum occurring in November 21-23, 2013). The possible causes for underestimation are meteorological field deviations (an overestimate in temperature and wind speed and an underestimate in humidity; Table S3) and emission errors. Anthropogenic emissions for $PM_{2.5}$ precursors used here are for the year 2017 over Central China from SEEA inventory (Table S4). From 2013 to 2017, anthropogenic NO_x, SO_2, and primary $PM_{2.5}$ emissions in Central China have declined substantially (Table S4), due to implementation of stringent emission control measures for the 12th-13th Five-Year Plans (Zheng et al., 2018). The anthropogenic emissions biases may affect our simulations and $PM_{2.5}$ attribution results to some extent. Aditionally, the underestimation is on a national scale when compared with the MEE observations, with a bias of -29.3 μg/m^3, -18.7 μg/m^3, -39.0 μg/m^3 and -21.4 μg/m^3 on average for SW-type, NW-type, A-type and C-type synoptic controlled episodes, respectively (Fig. 6). The national negative biases may be also attributed to insufficient resolution of the model (Yan et al., 2014) and imperfect chemical mechanisms (Yan et al., 2019). Nevertheless, the model can reproduce the evolution of each severe particle pollution episode well, including the accumulation of pollutants, the continuing process and the gradual dissipation of pollution (Fig. 5a/Fig. S1a).

Table 2

In order to examine the model performances in the $PM_{2.5}$ chemical compositions, we have reviewed the reported concentrations of $PM_{2.5}$ and the three inorganic salts (sulfate, nitrate and ammonium) in other cities (Table 4). The contributions of sulfate, nitrate and ammonium are 9.1%-31.9%, 5.7%-32.1% and 5.9%-13.3%, respectively. Figure S8/S9 shows the modeled spatial distribution of $PM_{2.5}$, sulfate, nitrate and ammonium concentrations averaged in the four typical heavy pollution processes over Jingzhou/China. The fractions of each inorganic salt to $PM_{2.5}$ for these four heavy pollution episodes are also shown in Fig. S10. Over Central China, the main components of $PM_{2.5}$ are the three inorganic salts in these pollution episodes, with the averaged contributions of sulfate, nitrate and ammonium being ~20%, ~18% and ~13%, respectively (Table 3). Our modelling results are comparable to the previous observed results (Table 4). Huang et al. (2014) have also reported that the three secondary inorganic particles rank the highest fraction among the $PM_{2.5}$ species in Central-Eastern China. As shown in Table 3, in addition to inorganic salts, other chemical components include dust (~15%), black carbon (~7%), primary organic aerosol (~14%) and second organic aerosol (~13%). In these four pollution events, the differences in mass percentages of each chemical component ranged from 0.1% (dust) to 6.2% (sulfate) (Table 3). See details in Sect. 3.4 for further analysis of the causes for the differences.

Table 3

Table 4

3.4 Local emissions versus transmission contributions to $PM_{2.5}$ under the four main PSCs

In order to investigate the effectiveness of emission control to reduce $PM_{2.5}$ pollution of Central China in the four typical severe particle pollution episodes, firstly

386 we estimate the local sources versus transmission contributions of $PM_{2.5}$ by GEOS-
387 Chem sensitivity simulations (Table 2). Results of XJ0 (Emissions outside Jingzhou are
388 zero) indicates the contribution of local emission sources to the $PM_{2.5}$ pollution over
389 Jingzhou. The difference between CON and XCC0 (Emissions outside Central China
390 are zero) shows the transmission contribution of $PM_{2.5}$ outside Central China to
391 Jingzhou. The difference between CON and NCP0/YRD0/PRD0/SCB0 (Emissions
392 over NCP/YRD/PRD/SCB are zero) represents the contribution of pollution transport
393 from NCP/YRD/PRD/SCB regions to Jingzhou.
394
395 Figure 7
396
397 For the SW-type synoptic situation, differences between the simulation results of
398 NCP0/YRD0/SCB0 and CON show that pollution controlled by SW-type circulation
399 over Central China is almost not affected by the emission sources from North
400 China/East China/Sichuan Basin. The concentrations of $PM_{2.5}$ and three inorganic salts
401 simulated by NCP0/YRD0/SCB0 are similar to those simulated by CON, with a
402 difference less than 3.0% (Fig. 8). However, affected by the southerly airflow at 850
403 hPa (Fig. 7), air pollutants formed over southern China could be transmitted to Central
404 China, with the transport contribution of 7.6%. In addition, the contributions from
405 transboundary transport from non-Jingzhou Central China is simulated to be 12.0% by
406 comparing the results of XJ0 and XCC0. The transport of air pollutants from the south
407 leads to the smallest proportion of the three inorganic salts (45.7%) in Jingzhou among
408 the four pollution episodes (50.3%-55.5% for other three episodes), because the
409 emissions of SO_2, NO_2 and NH_3 in the south (especially in Guangxi and Guizhou
410 province) are smaller than those in Central China (Li et al., 2017a). Associated with the
411 small surface wind speed of 2.1 m/s on average (Fig. 5) and the weak ascending in the
412 vertical direction (Fig. 7) at Jingzhou, it is not conducive to the dispersion of local
413 pollutants (Zheng et al., 2015). The high $PM_{2.5}$ concentrations are mainly accumulated

414 by local emissions. The simulations of XJ0 and CON show that local emission sources
415 over Jingzhou contribute ~70% to $PM_{2.5}$.
416
417 Figure 8
418 Figure 9
419
420 For the NW-type synoptic mode, affected by the northerly airflow (Fig. 9), it is
421 conducive to the southward movement of air pollutants in northern China (He et al.,
422 2018; Leung et al., 2018). Influenced by the local and surrounding terrain over Central
423 China (Fig. 1), two transmission channels are formed from north to south and from
424 northeast to southwest (Fig. 9). In addition, due to the local small wind speed (1.4 m/s
425 on average) near the ground (Fig. 5), the weak convection and the warm ridge along
426 the East Asia coast (Fig. 9), the local and transported pollutants accumulate in Central
427 China. The average concentration of $PM_{2.5}$ in Jingzhou is 179.4 $\mu g/m^3$. Due to the
428 transport contribution of pollutants from northern China (with much higher
429 anthropogenic emissions of SO_2, NO_2 and NH_3) (Li et al., 2017a), the total proportion
430 of the three inorganic salts is the highest (55.5%). The $PM_{2.5}$ concentration simulated
431 in NCP0 is 63.1% of that by CON simulation (Fig. 8), indicating that the transmission
432 contribution from North China in this heavy pollution episode is as high as 36.9%. The
433 contribution of local emission sources is much smaller than that of SW-type synoptic
434 pattern, only 41.2% (comparison between XJ0 and CON).
435
436 Figure 10
437
438 Under the A-type circulation, Jingzhou is controlled by a high pressure system
439 (Fig. 10) which can lead to stable weather conditions caused by radiation inversion
440 (Guo et al., 2015) and subsidence inversion (Kurita et al., 1985), being favorable to
441 continuous accumulation of local pollutants (Guo et al., 2015). The distribution of $PM_{2.5}$

in China is similar to that of SW-type weather condition, with an averaged $PM_{2.5}$ concentration of 128.6 μg/m^3 over Central China. Unlike SW-type, the $PM_{2.5}$ at Jingzhou in this synoptic pattern is less affected by transboundary transport, with the total transport contribution of the surrounding four major pollution regions being less than 9%. The contribution of local emission sources is about 82% (Fig. 8).

Figure 11

Under the C-type synoptic pattern, the southwest low pressure center is formed at 850 hPa, and Jingzhou is located in the low pressure system of the SLP field (Fig. 11). In combination with the large relative humidity (78% on average; Fig. 5; because that the occurrence season of C-type is the late winter and early spring), it can promote the haze pollution due to its impact on hydrophilic aerosols (Twohy et al., 2009; Zheng et al., 2015). Together with the small wind speed (less than 4 m/s; Fig. 5), it is easy to cause the accumulation of pollutants. The average concentration of $PM_{2.5}$ over Central China is as high as 203.7 μg/m^3. Air pollution controlled by this weather condition is the most serious of the four typical synoptic controls. However, in this weather situation, pollutants in North China are easy to diffuse (Miao et al., 2017; Li et al., 2019), and the concentration of $PM_{2.5}$ is significantly lower than that in the former three weather situations (Fig. 11 and Fig. S9). The contribution of pollution transport from non-Central China region simulated by GEOS-Chem is less than 8%, and the contribution of local emission sources at Jingzhou is more than 85% (Fig. 7).

3.5 Effectiveness of emission reduction under the four main PSCs

In order to estimate the effectiveness of emission reduction in severe pollution events forced by the four potential synoptic controls, we conduct sensitivity simulations by applying seven emission scenarios (Table 2). All emission scenarios use the reduction ratio of 20% which is close to the average of the target emission reduction of

all provinces in the 13th Five-year plan (The State Council of the People's Republic of China, 2016). Although the base year of emission reduction is 2015 for the 13th Five-year plan, it does not affect to use the simulation results of emission scenarios (with the reduction ratio of 20% applied to the simulated year 2013/2014) to explore the emission reduction effect of specific haze pollution events. The differences in model results between CON (control simulation) and JSN/JSNN/JALL (emissions of SO_2+NO_x/SO_2+NO_x+NH_3/all pollution sources at Jingzhou are reduced by 20%) represent the environmental benefits caused by different local emission reduction scenarios. The potential $PM_{2.5}$ mitigations by joint prevention and control in different regions are calculated by sensitivity experiments of CCALL (emissions of all pollution sources over Central China are reduced by 20%), CNALL (over Central China and NCP region), CPALL (over Central China and PRD region) and TALL (over Central China, NCP, YRD, PRD and SCB regions).

In the JSN emission reduction scenario, the sulfate and ammonium concentrations over Jingzhou are significantly reduced by 3.2-5.8 μg/m^3 (12.7-14.5%) and 0.6-1.9 μg/m^3 (3.2-5.9%) in these four pollution events, respectively. However, the concentration of nitrate increases (1.3-1.7%). This is because there is a competition mechanism between nitrate and sulfate. Ammonium ions always react with sulfate ions first to generate ammonium sulfate, which will continue to react with nitrate ions to generate ammonium nitrate when ammonium ions are rich (Mao et al., 2010). Thus the reduction of SO_2 emission increases the concentration of nitrate, which offset the contribution of sulfate particle reduction to the environment to some extent. Therefore, the application of JSN emission reduction scheme only reduces the $PM_{2.5}$ concentrations by 3.1-7.2 μg/m^3 (2.0-3.5%, Fig. 12). This inefficient emission reduction scheme is most widely used in heavy pollution areas over China in the past decade, ignoring the synergistic effect of various precursors.

Figure 12

By applying the JSNN and JALL emission reduction scenarios, we aim to evaluate the synergistic effect of multiple precursors on emission reduction. These two scenarios reduce the average sulfate concentration in Jingzhou by 2.8-6.7 μg/m^3 (11.3-17.3%) and 2.9-7.2 μg/m^3 (11.7-17.9%), and the ammonium concentration by 2.0-4.8 μg/m^3 (12.1-16.5%) and 2.2-4.7 μg/m^3 (13.2-17.3%), respectively. Unlike the increments of nitrate in JSN emission reduction scenario, the nitrate decreases (JSNN: 0.3-1.2 μg/m^3; JALL: 0.4-1.5 μg/m^3). Therefore, through the application of JSNN and JALL emission reduction schemes, $PM_{2.5}$ concentrations decrease by 4.9-8.3% and 9.0-15.9%, respectively (Fig. 12), much higher than the improvement by JSN scenario. Zheng et al. (2019b) has also evaluated the sensitiveness of NH_3 control to $PM_{2.5}$ reduction based on observations. However, these results indicate that it is unrealistic to substantially reduce local emissions to achieve the national air quality standard in the long term.

Additionally, the sensitivity simulations by excluding emission sources over upwind regions are conducted to estimate the potential $PM_{2.5}$ mitigations of inter-regional and intra-regional joint control. Our results show that after applying TALL emission reduction scenario, $PM_{2.5}$ concentrations have been significantly improved, with the improvement rates increased from 9.0-15.9% (by JALL scenario) to 17.4-18.8% (Fig. 12). Especially, the NW-type synoptic controlled air pollution episode shows the best effect of joint prevention, followed by SW-type. For NW-type, by reducing emissions over Central China and Northern China (CNALL scheme), $PM_{2.5}$ concentrations are reduced by 26.5 μg/m^3 (16.9%), much more effective than JALL emission reduction scheme (14.1 μg/m^3, 9.0%). In SW-type controlled pollution episode, it should be otherwise to decrease the emissions over Southern China in addition to Central China.

4. Conclusion

The $PM_{2.5}$ pollution in autumn and winter haze periods is now the key obstacle for further improving air quality in China. The extremely severe and persistent $PM_{2.5}$ pollution episodes are attributed to adverse synoptic conditions in addition to high precursor emissions. For the $PM_{2.5}$ mitigations during winter haze episodes in specific region forced by various potential synoptic controls, how to effectively reduce emissions has become an urgent scientific question to be answered. Our results over Central China could provide reference for regional air quality policy-making.

Through Lamb-Jenkension circulation classification, the top four potential synoptic controls of heavy $PM_{2.5}$ pollution days (totally 109 days) over Central China from 2013 to 2018 are decomposed to be SW-type, NW-type A-type and C-type, accounting for 29%, 27%, 19% and 12% of the total pollution days, respectively. In these four PSCs, three inorganic salt aerosols (sulfate: ~20%; nitrate: ~18%; ammonium: ~13%) totally accounted for ~51% of $PM_{2.5}$ concentrations simulated by optimized GEOS-Chem modelling.

In the SW-type/NW-type synoptic situation, affected by the southerly/northerly airflow, pollutants over southern/northern China could be transmitted to Central China, with the transport contribution of 7.6%/37%. In the situation A-type/C-type weather, affected by stable weather condition/high relative humidity, the pollution processes are less affected by the emission sources from non-local regions. And the local emission sources dominate the contribution (82%/85%) to $PM_{2.5}$.

By only reducing SO_2 and NO_x emission and not controlling NH_3, due to the competition mechanism between nitrate and sulfate, the concentrations of sulfate and ammonium decrease, but the concentration of nitrate increases instead. The enhanced nitrate counteracts the effect of sulfate reduction on $PM_{2.5}$ mitigations, with less than 4% decrease in $PM_{2.5}$. Even if the NH_3 emission is also reduced, the $PM_{2.5}$ concentration reduction is less than 9%. By applying the TALL emission reduction scenario, $PM_{2.5}$ concentrations would decrease significantly, with the improvement rate increased from 9.0-15.9% (by JALL scenario) to 17.4-18.8%.

These results provide an opportunity to effectively mitigate haze pollution by local emission control actions in coordination with regional collaborative actions according to different synoptic patterns. Especially, the NW-type synoptic controlled air pollution episode shows the best effect of joint prevention, followed by SW-type. It is noted that in this study, the division of transmission areas is relatively rough, and more accurate source area identification and refined assessment of emission reduction effect of multiple pollutants from source groups are needed in the follow-up.

Acknowledgement

This study was financially supported by the National Natural Science Foundation of China (41830965; 41775115; 41905112), the Key Program of Ministry of Science and Technology of the People's Republic of China (2017YFC0212602; 2016YFA0602002), the Key Program for Technical Innovation of Hubei Province (2017ACA089), the Program for Environmental Protection in Hubei Province (2017HB11) and the China Postdoctoral Science Foundation funded project (258572). The research was also funded by the Fundamental Research Funds for the Central Universities, China University of Geosciences (Wuhan) (G1323519230; 201616; 26420180020; CUG190609) and the Start-up Foundation for Advanced Talents (162301182756).

Author contributions

Yingying Yan and Shaofei Kong conceived and designed the research. Yingying Yan performed the data processing, model simulations, and analyses. Yue Zhou assisted in the circulation classification. Jian Wu provided the emission data over Central China. Shaofei Kong, Tianliang Zhao and Dantong Liu contributed the funding acquisition. Yingying Yan wrote the paper with input from all authors.

Data availability

Observational data are obtained from individual sources (see links in the text). Model results are available upon request. Model codes are available on a collaborative basis.

Competing interests

The authors declare that they have no conflict of interest.

References

The People's Government of Beijing Municipality (PGBM): Emergency plan for severe air pollution in Beijing, available at: http://www.beijing.gov.cn/zhengce/zhengcefagui/201905/t20190522_61613.html (last access: 14 July 2018), 2018 (in Chinese).

The People's Government of Guangdong Province (PGGP): Emergency plan for severe air pollution in Pearl River Delta, available at: http://www.gd.gov.cn/gkmlpt/content/0/142/post_142657.html#7 (last access: 14 July 2018), 2014 (in Chinese).

The People's Government of Shanghai Municipality (PGSM): Special emergency plan for heavy air pollution in Shanghai, available at: http://www.shanghai.gov.cn/nw2/nw2314/nw2319/nw31973/nw32019/nw32022/nw32023/u21aw1316153.html (last access: 14 July 2018), 2018 (in Chinese).

The State Council of the People's Republic of China (SCPPC): The Thirteenth Five-Year Plan for Energy Saving and Emission Reduction, available at: http://www.gov.cn/gongbao/content/2017/content_5163448.htm (last access: 14 July 2018), 2016 (in Chinese).

The State Council of the People's Republic of China (SCPPC): Air Pollution Prevention and Control Action Plan, available at: http://www.gov.cn/zhengce/content/2013-09/13/content_4561.htm (last access: 14 July 2018), 2013 (in Chinese).

Jenkinson A. F., Collison F. P.: An initial climatology of gales over the North Sea. Synoptic Climatology Branch Memorandum, 62. Bracknell: Meteorological Office, 1-18, 1977.

Lamb H H. Types and spells of weather around the year in the British Isles. Quarterly Journal Royal Meteorological Society, 76, 393-438, 1950.

Agarwal, N. K., Sharma, P., and Agarwal, S. K.: Particulate matter air pollution and cardiovascular disease, Medical Science, 21, 270-279, 2017.

An, Z., Huang, R.J., Zhang, R., Tie, X., Li, G., Cao, J., Zhou, W., Shi, Z., Han, Y., Gu, Z., and Ji, Y.: Severe haze in northern China: A synergy of anthropogenic emissions and atmospheric processes, Proceedings of the National Academy of Sciences of the United States of America, 116, 8657-8666, 10.1073/pnas.1900125116, 2019.

Bei, N., Zhao, L., Xiao, B., Meng, N., and Feng, T.: Impacts of local circulations on the wintertime air pollution in the Guanzhong Basin, China, Science of the Total Environment, 592, 373-390, 10.1016/j.scitotenv.2017.02.151, 2017.

Bi, X., Dai, Q., Wu, J., Zhang, Q., Zhang, W., Luo, R., Cheng, Y., Zhang, J., Wang, L., Yu, Z., Zhang, Y., Tian, Y., and Feng, Y.: Characteristics of the main primary source profiles of particulate matter across China from 1987 to 2017, Atmospheric Chemistry and Physics, 19, 3223-3243, 10.5194/acp-19-3223-2019, 2019.

Cheng, J., Su, J., Cui, T., Li, X., Dong, X., Sun, F., Yang, Y., Tong, D., Zheng, Y., Li, Y., Li, J., Zhang, Q., and He, K.: Dominant role of emission reduction in $PM_{2.5}$ air quality improvement in Beijing during 2013-2017: a model-based decomposition analysis, Atmospheric Chemistry and Physics, 19, 6125-6146, 10.5194/acp-19-6125-2019, 2019.

Cheng, Z., Luo, L., Wang, S., Wang, Y., Sharma, S., Shimadera, H., Wang, X., Bressi, M., de Miranda, R. M., Jiang, J., Zhou, W., Fajardo, O., Yan, N., and Hao, J.: Status and characteristics of ambient $PM_{2.5}$ pollution in global megacities, Environment International, 89-90, 212-221, 10.1016/j.envint.2016.02.003, 2016.

Chuang, M.T., Chiang, P.C., Chan, C.C., Wang, C.F., Chang, E. E., and Lee, C.T.: The effects of synoptical weather pattern and complex terrain on the formation of aerosol events in the Greater Taipei area, Science of the Total Environment, 399, 128-146, 10.1016/j.scitotenv.2008.01.051, 2008.

Geng, G., Xiao, Q., Zheng, Y., Tong, D., Zhang, Y., Zhang, X., Zhang, Q., He, K., and Liu, Y.: Impact of China's Air Pollution Prevention and Control Action Plan on $PM_{2.5}$ chemical composition over eastern China, Science China-Earth Sciences, 62, 1872-1884, 10.1007/s11430-018-9353-x, 2019.

Gong, W., Zhang, T., Zhu, Z., Ma, Y., Ma, X., and Wang, W.: Characteristics of $PM_{1.0}$, $PM_{2.5}$, and PM_{10}, and Their Relation to Black Carbon in Wuhan, Central China, Atmosphere, 6, 1377-1387, 10.3390/atmos6091377, 2015.

Guo, L., Guo, X., Fang, C., and Zhu, S.: Observation analysis on characteristics of formation, evolution and transition of a long-lasting severe fog and haze episode in North China, Science China-Earth Sciences, 58, 329-344, 10.1007/s11430-014-4924-2, 2015.

He, J., Gong, S., Zhou, C., Lu, S., Wu, L., Chen, Y., Yu, Y., Zhao, S., Yu, L., and Yin, C.: Analyses of winter circulation types and their impacts on haze pollution in

652 Beijing, Atmospheric Environment, 192, 94-103, 10.1016/j.atmosenv.2018.08.060,
653 2018.
654 Huang, R.J., Zhang, Y., Bozzetti, C., Ho, K.F., Cao, J.J., Han, Y., Daellenbach, K. R.,
655 Slowik, J. G., Platt, S. M., Canonaco, F., Zotter, P., Wolf, R., Pieber, S. M., Bruns,
656 E. A., Crippa, M., Ciarelli, G., Piazzalunga, A., Schwikowski, M., Abbaszade, G.,
657 Schnelle-Kreis, J., Zimmermann, R., An, Z., Szidat, S., Baltensperger, U., El
658 Haddad, I., and Prevot, A. S. H.: High secondary aerosol contribution to particulate
659 pollution during haze events in China, Nature, 514, 218-222, 10.1038/nature13774,
660 2014.
661 Huang, X., Ding, A., Gao, J., Zheng, B., Zhou, D., Qi, X., Tang, R., Wang, J., Ren, C.,
662 Nie, W., Chi, X., Xu, Z., Chen, L., Li, Y., Che, F., Pang, N., Wang, H., Tong, D.,
663 Qin, W., Cheng, W., Liu, W., Fu, Q., Liu, B., Chai, F., Davis, S. J., Zhang, Q., and
664 He, K.: Enhanced secondary pollution offset reduction of primary emissions during
665 COVID-19 lockdown in China, National Science Review, 10.1093/nsr/nwaa137,
666 2020.
667 Kurita, H., Sasaki, K., Muroga, H., Ueda, H., and Wakamatsu, S.: Long-range transport
668 of air pollution under light gradient wind conditions, Journal of Climate and Applied
669 Meteorology, 24, 425-434, 10.1175/1520-0450(1985)024<0425:lrtoap>2.0.co;2,
670 1985.
671 Leung, D. M., Tai, A. P. K., Mickley, L. J., Moch, J. M., van Donkelaar, A., Shen, L.,
672 and Martin, R. V.: Synoptic meteorological modes of variability for fine particulate
673 matter ($PM_{2.5}$) air quality in major metropolitan regions of China, Atmospheric
674 Chemistry and Physics, 18, 6733-6748, 10.5194/acp-18-6733-2018, 2018.
675 Li, J., Liao, H., Hu, J., and Li, N.: Severe particulate pollution days in China during
676 2013-2018 and the associated typical weather patterns in Beijing-Tianjin-Hebei and
677 the Yangtze River Delta regions, Environmental Pollution, 248, 74-81,
678 10.1016/j.envpol.2019.01.124, 2019.
679 Li, M., Zhang, Q., Kurokawa, J.-i., Woo, J.-H., He, K., Lu, Z., Ohara, T., Song, Y.,
680 Streets, D. G., Carmichael, G. R., Cheng, Y., Hong, C., Huo, H., Jiang, X., Kang, S.,
681 Liu, F., Su, H., and Zheng, B.: MIX: a mosaic Asian anthropogenic emission
682 inventory under the international collaboration framework of the MICS-Asia and
683 HTAP, Atmospheric Chemistry and Physics, 17, 935-963, 10.5194/acp-17-935-
684 2017, 2017a.
685 Li, X., Zhang, Q., Zhang, Y., Zhang, L., Wang, Y., Zhang, Q., Li, M., Zheng, Y., Geng,
686 G., Wallington, T. J., Han, W., Shen, W., and He, K.: Attribution of $PM_{2.5}$ exposure
687 in Beijing-Tianjin-Hebei region to emissions: implication to control strategies,
688 Science Bulletin, 62, 957-964, 10.1016/j.scib.2017.06.005, 2017b.

Li, Z., Guo, J., Ding, A., Liao, H., Liu, J., Sun, Y., Wang, T., Xue, H., Zhang, H., and Zhu, B.: Aerosol and boundary-layer interactions and impact on air quality, National Science Review, 4, 810-833, 10.1093/nsr/nwx117, 2017c.

Liao, Z., Gao, M., Sun, J., and Fan, S.: The impact of synoptic circulation on air quality and pollution-related human health in the Yangtze River Delta region, Science of the Total Environment, 607, 838-846, 10.1016/j.scitotenv.2017.07.031, 2017.

Liao, Z., Xie, J., Fang, X., Wang, Y., Zhang, Y., Xu, X., and Fan, S.: Modulation of synoptic circulation to dry season $PM_{2.5}$ pollution over the Pearl River Delta region: An investigation based on self-organizing maps, Atmospheric Environment, 230, 10.1016/j.atmosenv.2020.117482, 2020.

Lin, Y., Zou, J., Yang, W., and Li, C.Q.: A Review of Recent Advances in Research on $PM_{2.5}$ in China, International Journal of Environmental Research and Public Health, 15, 10.3390/ijerph15030438, 2018.

Liu, M., Huang, X., Song, Y., Tang, J., Cao, J., Zhang, X., Zhang, Q., Wang, S., Xu, T., Kang, L., Cai, X., Zhang, H., Yang, F., Wang, H., Yu, J. Z., Lau, A. K. H., He, L., Huang, X., Duan, L., Ding, A., Xue, L., Gao, J., Liu, B., and Zhu, T.: Ammonia emission control in China would mitigate haze pollution and nitrogen deposition, but worsen acid rain, Proceedings of the National Academy of Sciences of the United States of America, 116, 7760-7765, 10.1073/pnas.1814880116, 2019.

Mao, J., Jacob, D. J., Evans, M. J., Olson, J. R., Ren, X., Brune, W. H., Clair, J. M. S., Crounse, J. D., Spencer, K. M., Beaver, M. R., Wennberg, P. O., Cubison, M. J., Jimenez, J. L., Fried, A., Weibring, P., Walega, J. G., Hall, S. R., Weinheimer, A. J., Cohen, R. C., Chen, G., Crawford, J. H., McNaughton, C., Clarke, A. D., Jaeglé, L., Fisher, J. A., Yantosca, R. M., Le Sager, P., and Carouge, C.: Chemistry of hydrogen oxide radicals (HOx) in the Arctic troposphere in spring, Atmospheric Chemistry and Physics, 10, 5823-5838, 10.5194/acp-10-5823-2010, 2010.

Miao, Y., Guo, J., Liu, S., Liu, H., Li, Z., Zhang, W., and Zhai, P.: Classification of summertime synoptic patterns in Beijing and their associations with boundary layer structure affecting aerosol pollution, Atmospheric Chemistry and Physics, 17, 3097-3110, 10.5194/acp-17-3097-2017, 2017.

Ning, G., Wang, S., Yim, S. H. L., Li, J., Hu, Y., Shang, Z., Wang, J., and Wang, J.: Impact of low-pressure systems on winter heavy air pollution in the northwest Sichuan Basin, China, Atmospheric Chemistry and Physics, 18, 13601-13615, 10.5194/acp-18-13601-2018, 2018.

Pope, R. J., Savage, N. H., Chipperfield, M. P., Ordonez, C., and Neal, L. S.: The influence of synoptic weather regimes on UK air quality: regional model studies of

tropospheric column NO_2, Atmospheric Chemistry and Physics, 15, 11201-11215, 10.5194/acp-15-11201-2015, 2015.

Russo, A., Trigo, R. M., Martins, H., and Mendes, M. T.: NO_2, PM_{10} and O_3 urban concentrations and its association with circulation weather types in Portugal, Atmospheric Environment, 89, 768-785, 10.1016/j.atmosenv.2014.02.010, 2014.

Shu, L., Xie, M., Gao, D., Wang, T., Fang, D., Liu, Q., Huang, A., and Peng, L.: Regional severe particle pollution and its association with synoptic weather patterns in the Yangtze River Delta region, China, Atmospheric Chemistry and Physics, 17, 12871-12891, 10.5194/acp-17-12871-2017, 2017.

Sun, Y., Niu, T., He, J., Ma, Z., Liu, P., Xiao, D., Hu, J., Yang, J., and Yan, X.: Classification of circulation patterns during the formation and dissipation of continuous pollution weather over the Sichuan Basin, China, Atmospheric Environment, 223, 10.1016/j.atmosenv.2019.117244, 2020.

Sun, Y. L., Chen, C., Zhang, Y. J., Xu, W. Q., Zhou, L. B., Cheng, X. L., Zheng, H. T., Ji, D. S., Li, J., Tang, X., Fu, P. Q., and Wang, Z. F.: Rapid formation and evolution of an extreme haze episode in Northern China during winter 2015, Scientific Reports, 6, 10.1038/srep27151, 2016.

Tian, S. L., Pan, Y. P., and Wang, Y. S.: Size-resolved source apportionment of particulate matter in urban Beijing during haze and non-haze episodes, Atmospheric Chemistry and Physics, 16, 1-19, 10.5194/acp-16-1-2016, 2016.

Trigo, R. M., and DaCamara, C. C.: Circulation weather types and their influence on the precipitation regime in Portugal, International Journal of Climatology, 20, 1559-1581, 10.1002/1097-0088(20001115)20:13<1559::aid-joc555>3.0.co;2-5, 2000.

Twohy, C. H., Coakley, J. A., Jr., and Tahnk, W. R.: Effect of changes in relative humidity on aerosol scattering near clouds, Journal of Geophysical Research-Atmospheres, 114, 10.1029/2008jd010991, 2009.

Wang, X., Wei, W., Cheng, S., Li, J., Zhang, H., and Lv, Z.: Characteristics and classification of $PM_{2.5}$ pollution episodes in Beijing from 2013 to 2015, Science of the Total Environment, 612, 170-179, 10.1016/j.scitotenv.2017.08.206, 2018.

Wang, Y., Chen, Y., Wu, Z., Shang, D., Bian, Y., Du, Z., Schmitt, S. H., Su, R., Gkatzelis, G. I., Schlag, P., Hohaus, T., Voliotis, A., Lu, K., Zen, L., Zhao, C., Alfarra, M. R., McFiggans, G., Wiedensohler, A., Kiendler-Scharr, A., Zhang, Y., and Hu, M.: Mutual promotion between aerosol particle liquid water and particulate nitrate enhancement leads to severe nitrate-dominated particulate matter pollution and low visibility, Atmospheric Chemistry and Physics, 20, 2161-2175, 10.5194/acp-20-2161-2020, 2020.

Wu, J., Kong, S., Wu, F., Cheng, Y., Zheng, S., Yan, Q., Zheng, H., Yang, G., Zheng, M., Liu, D., Zhao, D., and Qi, S.: Estimating the open biomass burning emissions in central and eastern China from 2003 to 2015 based on satellite observation, Atmospheric Chemistry and Physics, 18, 11623-11646, 10.5194/acp-18-11623-2018, 2018.

Xu, G., Jiao, L., Zhang, B., Zhao, S., Yuan, M., Gu, Y., Liu, J., and Tang, X.: Spatial and temporal variability of the $PM_{2.5}/PM_{10}$ ratio in Wuhan, Central China, Aerosol and Air Quality Research, 17, 741-751, 10.4209/aaqr.2016.09.0406, 2017.

Yan, Q., Kong, S., Yan, Y., Liu, H., Wang, W., Chen, K., Yin, Y., Zheng, H., Wu, J., Yao, L., Zeng, X., Cheng, Y., Zheng, S., Wu, F., Niu, Z., Zhang, Y., Zheng, M., Zhao, D., Liu, D., and Qi, S.: Emission and simulation of primary fine and submicron particles and water-soluble ions from domestic coal combustion in China, Atmospheric Environment, 224, 10.1016/j.atmosenv.2020.117308, 2020.

Yan, Y., Cabrera-Perez, D., Lin, J., Pozzer, A., Hu, L., Millet, D. B., Porter, W. C., and Lelieveld, J.: Global tropospheric effects of aromatic chemistry with the SAPRC-11 mechanism implemented in GEOS-Chem version 9-02, Geoscientific Model Development, 12, 111-130, 10.5194/gmd-12-111-2019, 2019.

Yan, Y. Y., Lin, J. T., Kuang, Y., Yang, D., and Zhang, L.: Tropospheric carbon monoxide over the Pacific during HIPPO: two-way coupled simulation of GEOS-Chem and its multiple nested models, Atmospheric Chemistry and Physics, 14, 12649-12663, 10.5194/acp-14-12649-2014, 2014.

Yang, Y., Zheng, X., Gao, Z., Wang, H., Wang, T., Li, Y., Lau, G. N. C., and Yim, S. H. L.: Long-term trends of persistent synoptic circulation events in planetary boundary layer and their relationships with haze pollution in winter half year over Eastern China, Journal of Geophysical Research-Atmospheres, 123, 10991-11007, 10.1029/2018jd028982, 2018.

Yu, C., Zhao, T., Bai, Y., Zhang, L., Kong, S., Yu, X., He, J., Cui, C., Yang, J., You, Y., Ma, G., Wu, M., and Chang, J.: Heavy air pollution with a unique "non-stagnant" atmospheric boundary layer in the Yangtze River middle basin aggravated by regional transport of $PM_{2.5}$ over China, Atmospheric Chemistry and Physics, 20, 7217-7230, 10.5194/acp-20-7217-2020, 2020.

Zhang, J. P., Zhu, T., Zhang, Q. H., Li, C. C., Shu, H. L., Ying, Y., Dai, Z. P., Wang, X., Liu, X. Y., Liang, A. M., Shen, H. X., and Yi, B. Q.: The impact of circulation patterns on regional transport pathways and air quality over Beijing and its surroundings, Atmospheric Chemistry and Physics, 12, 5031-5053, 10.5194/acp-12-5031-2012, 2012.

797 Zhang, Q., Jiang, X., Tong, D., Davis, S. J., Zhao, H., Geng, G., Feng, T., Zheng, B.,
798 Lu, Z., Streets, D. G., Ni, R., Brauer, M., van Donkelaar, A., Martin, R. V., Huo, H.,
799 Liu, Z., Pan, D., Kan, H., Yan, Y., Lin, J., He, K., and Guan, D.: Transboundary
800 health impacts of transported global air pollution and international trade, Nature, 543,
801 10.1038/nature21712, 2017.
802 Zhang, Q., Zheng, Y., Tong, D., Shao, M., Wang, S., Zhang, Y., Xu, X., Wang, J., He,
803 H., Liu, W., Ding, Y., Lei, Y., Li, J., Wang, Z., Zhang, X., Wang, Y., Cheng, J., Liu,
804 Y., Shi, Q., Yan, L., Geng, G., Hong, C., Li, M., Liu, F., Zheng, B., Cao, J., Ding,
805 A., Gao, J., Fu, Q., Huo, J., Liu, B., Liu, Z., Yang, F., He, K., and Hao, J.: Drivers of
806 improved PM2.5 air quality in China from 2013 to 2017, Proceedings of the National
807 Academy of Sciences of the United States of America, 116, 24463-24469,
808 10.1073/pnas.1907956116, 2019.
809 Zheng, B., Tong, D., Li, M., Liu, F., Hong, C., Geng, G., Li, H., Li, X., Peng, L., Qi,
810 J., Yan, L., Zhang, Y., Zhao, H., Zheng, Y., He, K., and Zhang, Q.: Trends in China's
811 anthropogenic emissions since 2010 as the consequence of clean air actions,
812 Atmospheric Chemistry and Physics, 18, 14095-14111, 10.5194/acp-18-14095-
813 2018, 2018.
814 Zheng, H., Kong, S., Wu, F., Cheng, Y., Niu, Z., Zheng, S., Yang, G., Yao, L., Yan,
815 Q., Wu, J., Zheng, M., Chen, N., Xu, K., Yan, Y., Liu, D., Zhao, D., Zhao, T., Bai,
816 Y., Li, S., and Qi, S.: Intra-regional transport of black carbon between the south edge
817 of the North China Plain and central China during winter haze episodes, Atmospheric
818 Chemistry and Physics, 19, 4499-4516, 10.5194/acp-19-4499-2019, 2019a.
819 Zheng, M., Wang, Y., Bao, J., Yuan, L., Zheng, H., Yan, Y., Liu, D., Xie, M., and
820 Kong, S.: Initial Cost Barrier of Ammonia Control in Central China, Geophysical
821 Research Letters, 46, 14175-14184, 10.1029/2019gl084351, 2019b.
822 Zheng, X. Y., Fu, Y. F., Yang, Y. J., and Liu, G. S.: Impact of atmospheric circulations
823 on aerosol distributions in autumn over eastern China: observational evidence,
824 Atmospheric Chemistry and Physics, 15, 12115-12138, 10.5194/acp-15-12115-
825 2015, 2015.
826 Zhong, J., Zhang, X., Dong, Y., Wang, Y., Liu, C., Wang, J., Zhang, Y., and Che, H.:
827 Feedback effects of boundary-layer meteorological factors on cumulative explosive
828 growth of $PM_{2.5}$ during winter heavy pollution episodes in Beijing from 2013 to
829 2016, Atmospheric Chemistry and Physics, 18, 247-258, 10.5194/acp-18-247-2018,
830 2018.
831 Bai, Z., Winiwarter, W., Klimont, Z., Velthof, G., Misselbrook, T., Zhao, Z., Jin, X.,
832 Oenema, O., Hu, C., and Ma, L.: Further Improvement of Air Quality in China Needs

Clear Ammonia Mitigation Target, Environmental Science & Technology, 53, 10542-10544, 10.1021/acs.est.9b04725, 2019.

Xu, Z., Liu, M., Zhang, M., Song, Y., Wang, S., Zhang, L., Xu, T., Wang, T., Yan, C., Zhou, T., Sun, Y., Pan, Y., Hu, M., Zheng, M., and Zhu, T.: High efficiency of livestock ammonia emission controls in alleviating particulate nitrate during a severe winter haze episode in northern China, Atmospheric Chemistry and Physics, 19, 5605-5613, 10.5194/acp-19-5605-2019, 2019.

Ye, Z., Guo, X., Cheng, L., Cheng, S., Chen, D., Wang, W., and Liu, B.: Reducing PM2.5 and secondary inorganic aerosols by agricultural ammonia emission mitigation within the Beijing-Tianjin-Hebei region, China, Atmospheric Environment, 219, 10.1016/j.atmosenv.2019.116989, 2019.

Cao, J.-J., Shen, Z.-X., Chow, J. C., Watson, J. G., Lee, S.-C., Tie, X.-X., Ho, K.-F., Wang, G.-H., and Han, Y.-M.: Winter and Summer PM2.5 Chemical Compositions in Fourteen Chinese Cities, Journal of the Air & Waste Management Association, 62, 1214-1226, 10.1080/10962247.2012.701193, 2012.

Huang, W., Cao, J., Tao, Y., Dai, L., Lu, S.-E., Hou, B., Wang, Z., and Zhu, T.: Seasonal Variation of Chemical Species Associated With Short-Term Mortality Effects of PM2.5 in Xi'an, a Central City in China, American Journal of Epidemiology, 175, 556-566, 10.1093/aje/kwr342, 2012.

Liu, Z., Gao, W., Yu, Y., Hu, B., Xin, J., Sun, Y., Wang, L., Wang, G., Bi, X., Zhang, G., Xu, H., Cong, Z., He, J., Xu, J., and Wang, Y.: Characteristics of PM2.5 mass concentrations and chemical species in urban and background areas of China: emerging results from the CARE-China network, Atmospheric Chemistry and Physics, 18, 8849-8871, 10.5194/acp-18-8849-2018, 2018.

Luo, Y., Zhou, X., Zhang, J., Xiao, Y., Wang, Z., Zhou, Y., and Wang, W.: PM2.5 pollution in a petrochemical industry city of northern China: Seasonal variation and source apportionment, Atmospheric Research, 212, 285-295, 10.1016/j.atmosres.2018.05.029, 2018.

Wang, H. L., Qiao, L. P., Lou, S. R., Zhou, M., Ding, A. J., Huang, H. Y., Chen, J. M., Wang, Q., Tao, S., Chen, C. H., Li, L., and Huang, C.: Chemical composition of PM2.5 and meteorological impact among three years in urban Shanghai, China, Journal of Cleaner Production, 112, 1302-1311, 10.1016/j.jclepro.2015.04.099, 2016a.

Wang, J., Li, X., Zhang, W., Jiang, N., Zhang, R., and Tang, X.: Secondary PM2.5 in Zhengzhou, China: Chemical Species Based on Three Years of Observations, Aerosol and Air Quality Research, 16, 91-104, 10.4209/aaqr.2015.01.0007, 2016b.

869 Wang, Q., Fang, J., Shi, W., and Dong, X.: Distribution characteristics and policy-
870 related improvements of PM2.5 and its components in six Chinese cities,
871 Environmental Pollution, 266, 10.1016/j.envpol.2020.115299, 2020.
872 Xu, Q., Wang, S., Jiang, J., Bhattarai, N., Li, X., Chang, X., Qiu, X., Zheng, M., Hua,
873 Y., and Hao, J.: Nitrate dominates the chemical composition of PM2.5 during haze
874 event in Beijing, China, Science of the Total Environment, 689, 1293-1303,
875 10.1016/j.scitotenv.2019.06.294, 2019.
876 Zhang, T., Cao, J. J., Tie, X. X., Shen, Z. X., Liu, S. X., Ding, H., Han, Y. M., Wang,
877 G. H., Ho, K. F., Qiang, J., and Li, W. T.: Water-soluble ions in atmospheric aerosols
878 measured in Xi'an, China: Seasonal variations and sources, Atmospheric Research,
879 102, 110-119, 10.1016/j.atmosres.2011.06.014, 2011.
880 Zheng, J., Hu, M., Peng, J., Wu, Z., Kumar, P., Li, M., Wang, Y., and Guo, S.: Spatial
881 distributions and chemical properties of PM2.5 based on 21 field campaigns at 17
882 sites in China, Chemosphere, 159, 480-487, 10.1016/j.chemosphere.2016.06.032,
883 2016.
884 Chang, W., and Zhan, J.: The association of weather patterns with haze episodes:
885 Recognition by PM2.5 oriented circulation classification applied in Xiamen,
886 Southeastern China, Atmospheric Research, 197, 425-436,
887 10.1016/j.atmosres.2017.07.024, 2017.
888 Dai, H., Zhu, J., Liao, H., Li, J., Liang, M., Yang, Y., and Yue, X.: Co-occurrence of
889 ozone and PM2.5 pollution in the Yangtze River Delta over 2013-2019:
890 Spatiotemporal distribution and meteorological conditions, Atmospheric Research,
891 249, 10.1016/j.atmosres.2020.105363, 2021.
892 Ding, A., Huang, X., Nie, W., Chi, X., Xu, Z., Zheng, L., Xu, Z., Xie, Y., Qi, X., Shen,
893 Y., Sun, P., Wang, J., Wang, L., Sun, J., Yang, X.-Q., Qin, W., Zhang, X., Cheng,
894 W., Liu, W., Pan, L., and Fu, C.: Significant reduction of PM2.5 in eastern China
895 due to regional-scale emission control: evidence from SORPES in 2011-2018,
896 Atmospheric Chemistry and Physics, 19, 11791-11801, 10.5194/acp-19-11791-2019,
897 2019.
898 Fu, X., Wang, S., Xing, J., Zhang, X., Wang, T., and Hao, J.: Increasing Ammonia
899 Concentrations Reduce the Effectiveness of Particle Pollution Control Achieved via
900 SO2 and NOX Emissions Reduction in East China, Environmental Science &
901 Technology Letters, 4, 221-227, 10.1021/acs.estlett.7b00143, 2017.
902 Xing, J., Ding, D., Wang, S., Zhao, B., Jang, C., Wu, W., Zhang, F., Zhu, Y., and Hao,
903 J.: Quantification of the enhanced effectiveness of NOx control from simultaneous
904 reductions of VOC and NH3 for reducing air pollution in the Beijing-Tianjin-Hebei

region, China, Atmospheric Chemistry and Physics, 18, 7799-7814, 10.5194/acp-18-7799-2018, 2018.

Xing, J., Ding, D., Wang, S., Dong, Z., Kelly, J. T., Jang, C., Zhu, Y., and Hao, J.: Development and application of observable response indicators for design of an effective ozone and fine-particle pollution control strategy in China, Atmospheric Chemistry and Physics, 19, 13627-13646, 10.5194/acp-19-13627-2019, 2019.

Philipp, A., Beck, C., Huth, R., and Jacobeit, J.: Development and comparison of circulation type classifications using the COST 733 dataset and software, International Journal of Climatology, 36, 2673-2691, 10.1002/joc.3920, 2016.

Pope, R. J., Savage, N. H., Chipperfield, M. P., Arnold, S. R., and Osborn, T. J.: The influence of synoptic weather regimes on UK air quality: analysis of satellite column NO2, Atmospheric Science Letters, 15, 211-217, 10.1002/asl2.492, 2014.

Russo, A., Trigo, R. M., Martins, H., and Mendes, M. T.: NO2, PM10 and O3 urban concentrations and its association with circulation weather types in Portugal, Atmospheric Environment, 89, 768-785, 10.1016/j.atmosenv.2014.02.010, 2014.

Santurtun, A., Carlos Gonzalez-Hidalgo, J., Sanchez-Lorenzo, A., and Teresa Zarrabeitia, M.: Surface ozone concentration trends and its relationship with weather types in Spain (2001-2010), Atmospheric Environment, 101, 10-22, 10.1016/j.atmosenv.2014.11.005, 2015.

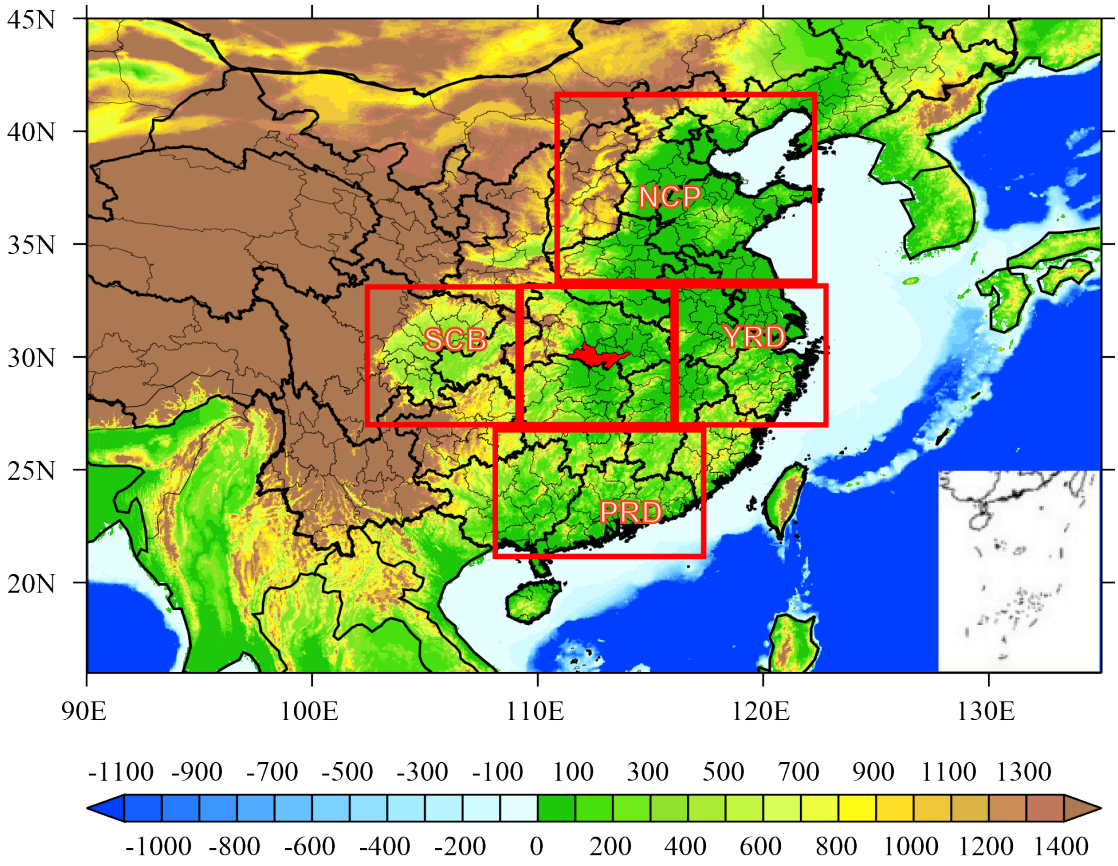

Figue 1 The location of Jingzhou (red area) and the major haze pollution regions of NCP, YRD, PRD, and SCB. The areas framed in red are used to investigate the inter-regional imapcts by GEOS-Chem sensitivity simulations. The overlaid map shows the surface elevation (m) from a 2 min Gridded Global Relief Data (ETOPO2v2) available at NGDC Marine Trackline Geophysical database (http://www.ngdc.noaa.gov/mgg/global/etopo2.html).

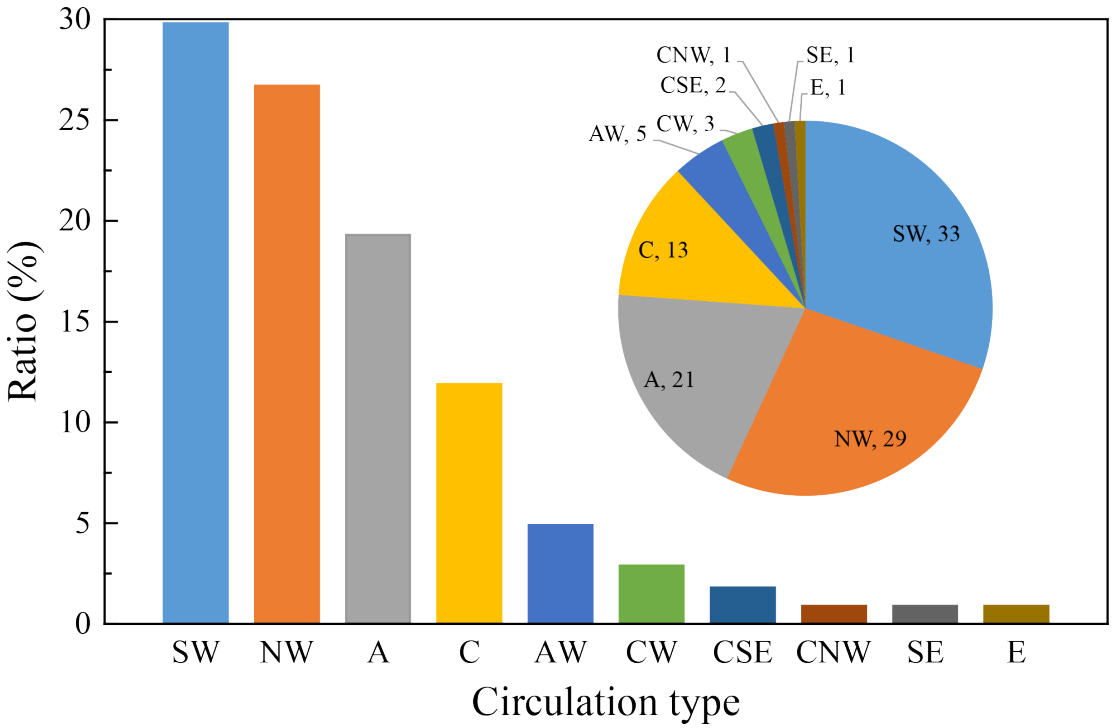

Figure 2 Frequency distributions of ten circulation types for the heavy pollution days of 2013-2018 over Jingzhou. The occurrence numbers of each type are shown. The ten circulation types include Southwest (SW), Northwest (NW), Anticyclone (A), Cyclone (C), Anticyclone-West (AW), Cyclone-West (CW), Cyclone-Southeast (CSE), Cyclone-Northwest (CNW), Southeast (SE) and East (E), respectively.

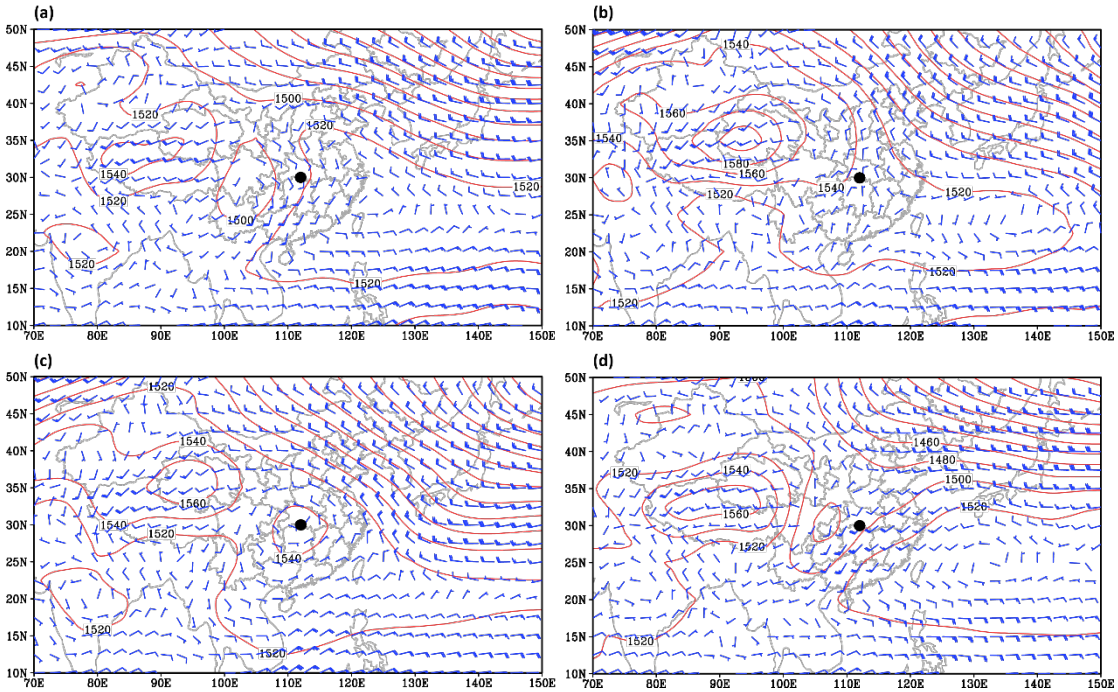

Figure 3 Spatial distribution of 850 hPa geopotential height and wind vector for SW-type (a), NW-type (b), A-type (c) and C-type (d) synoptic control averaged over 2013-2018. The black dot indicates the location of Jingzhou.

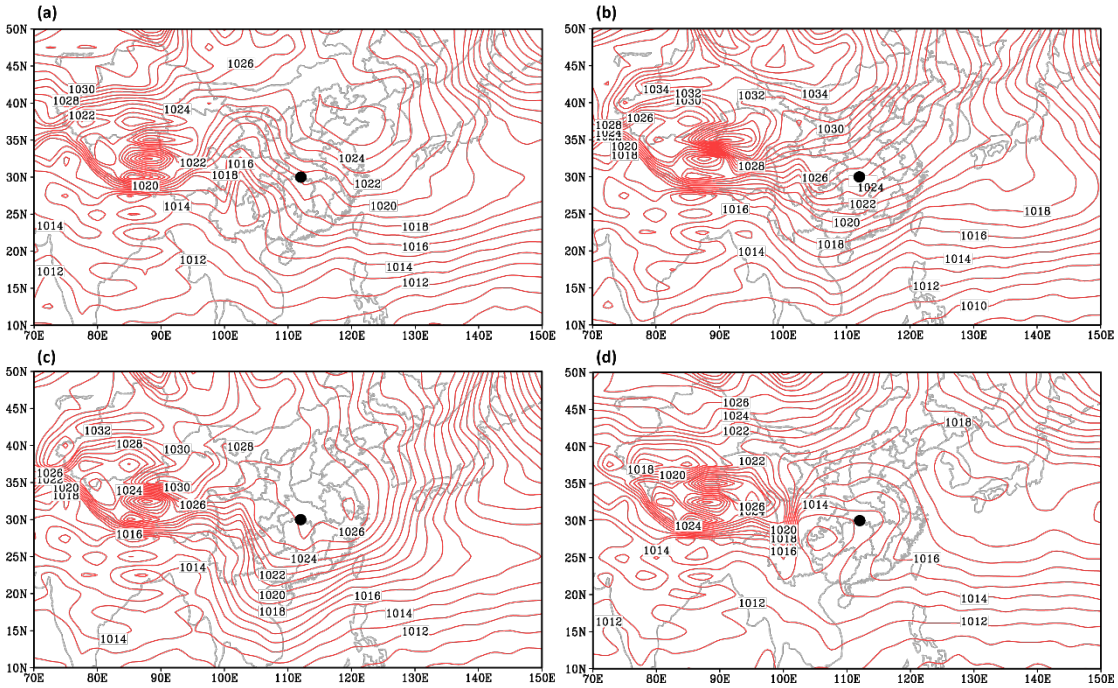

Figure 4 Spatial distribution of sea level pressure for SW-type (a), NW-type (b), A-type (c) and C-type (d) synoptic control averaged over 2013-2018. The black dot indicates the location of Jingzhou.

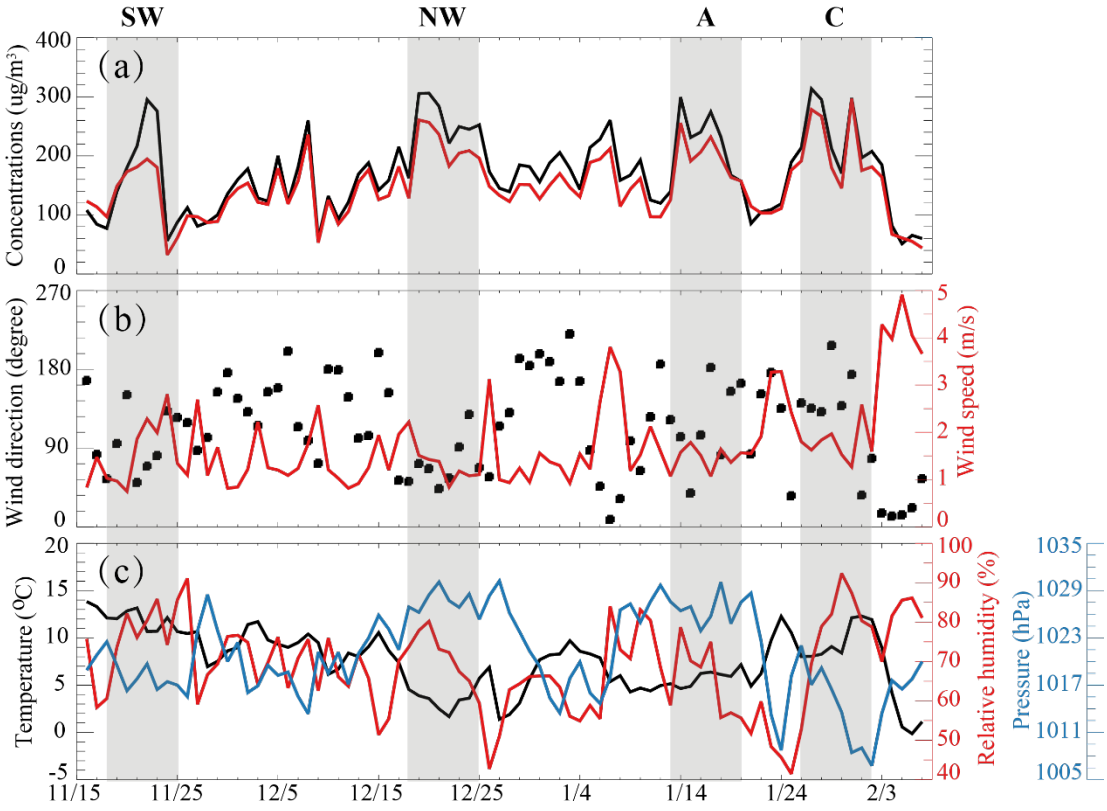

Figure 5 (a) Daily mean values of modeled (red line) and observed (black line) $PM_{2.5}$ concentration ($\mu g/m^3$) at Jingzhou and four severe pollution events (grey area) from November, 2013 to February, 2014. (b) Observed daily mean wind speed (red line) and wind direction (black dots). (c) Obseved temperature (black line), relative humidity (red line) and sea level pressure (blue line).

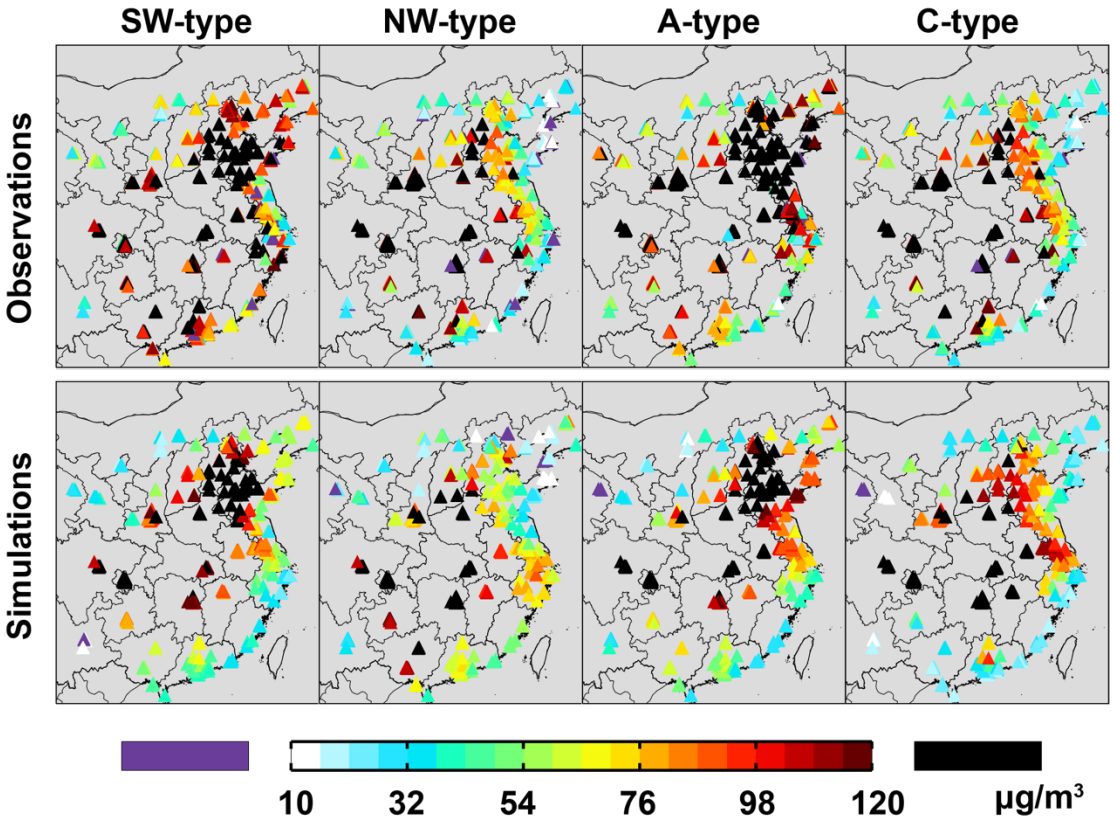

Figure 6 Spatial distribution of observed (top row) and modeled (bottom row, by CON case) $PM_{2.5}$ concentrations ($\mu g/m^3$) averaged over four severe pollution episodes controlled by SW-type (first column), NW-type (second column), A-type (third column) and C-type (forth column) synoptic pattern, respectively.

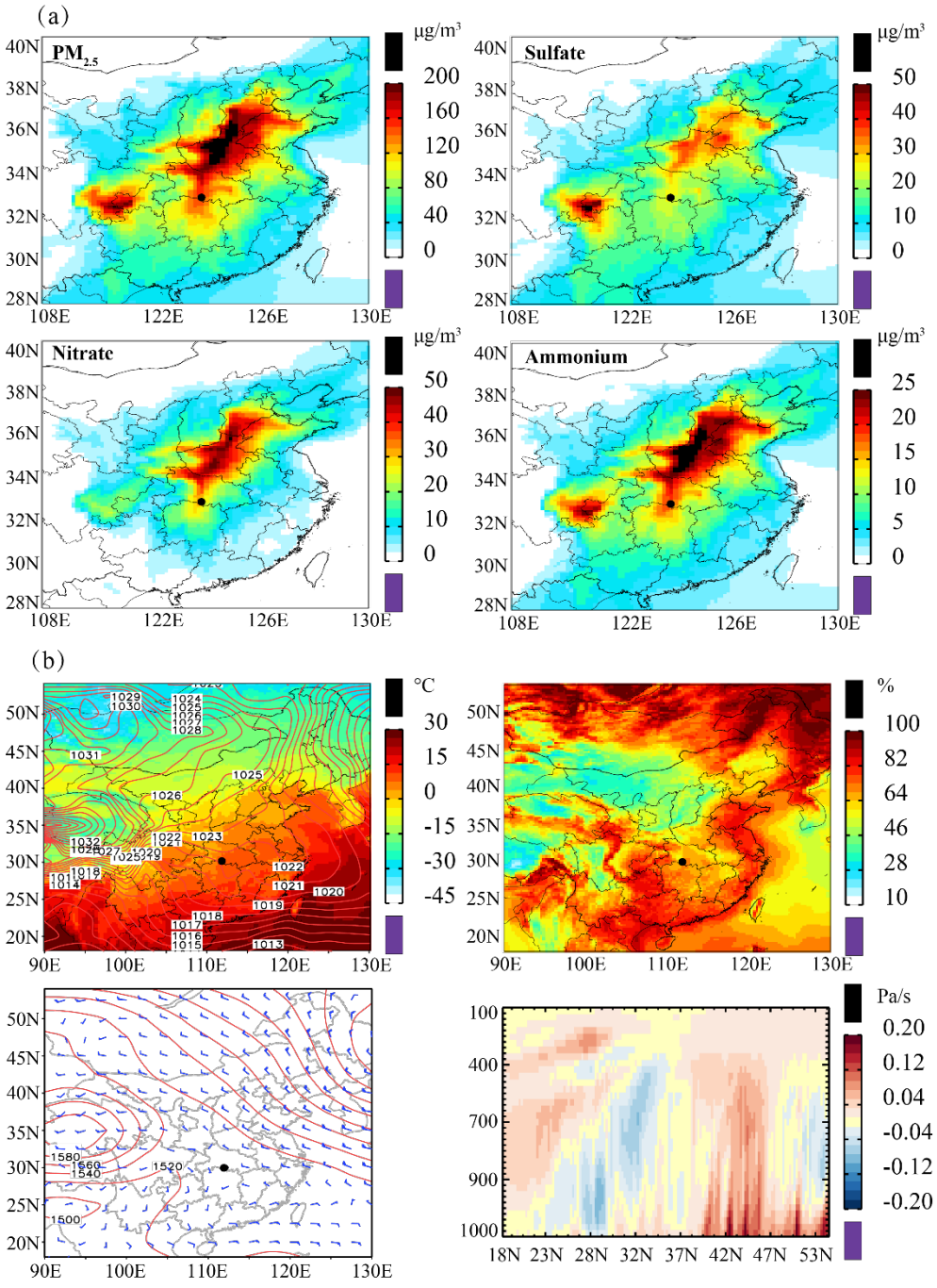

Figure 7 (a) Spatial distribution of $PM_{2.5}$, sulfate, nitrate and ammonium concentrations averaged over SW-type synoptic controls (18-25 November, 2013) simulated by GEOS-Chem control simulation (μg/m^3). (b) Meteorological conditions of SW-type: sea level pressure (red line) and temperature (colour shades), surface relative humidity (%) fields, 850 hPa wind and geopotential height (red line) and height–latitude cross-sections of vertical velocity (Pa/s).

980

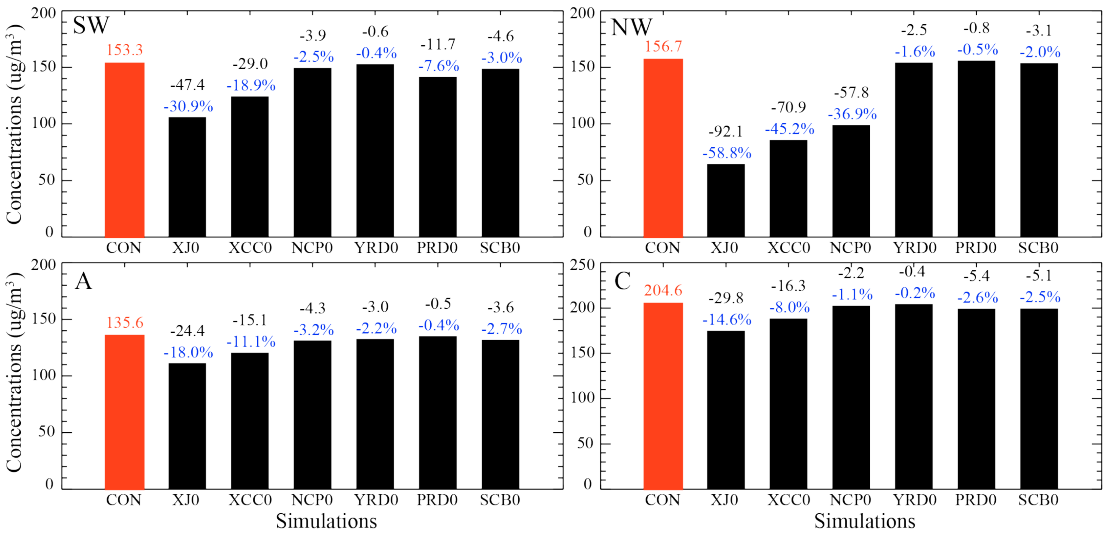

981

982 Figure 8 Modeled concentrations (μg/m^3) of $PM_{2.5}$ at Jingzhou in the GEOS-Chem
983 control (red bar) and sensitivity (black bar) simulations in view of the regional
984 transportation, and the differences (black characters for mass concentrations and blue
985 characters for mass percentages) between the sensitivity and the control simulations.
986 The abbreviations of each simulation referred to Table 2.

987

988

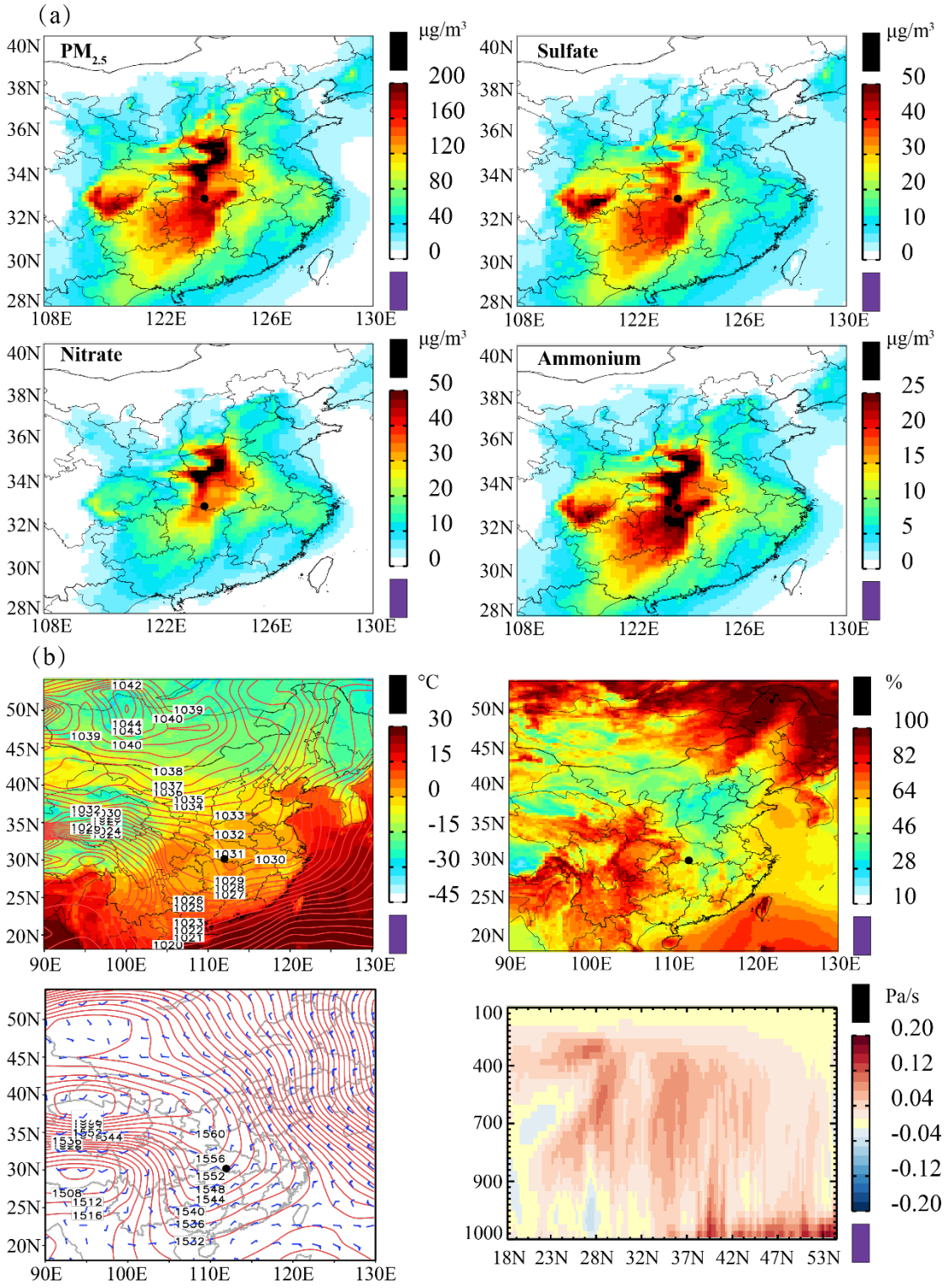

Figure 9 As in Fig. 6 but for NW-type synoptic control (19-26 December, 2013).

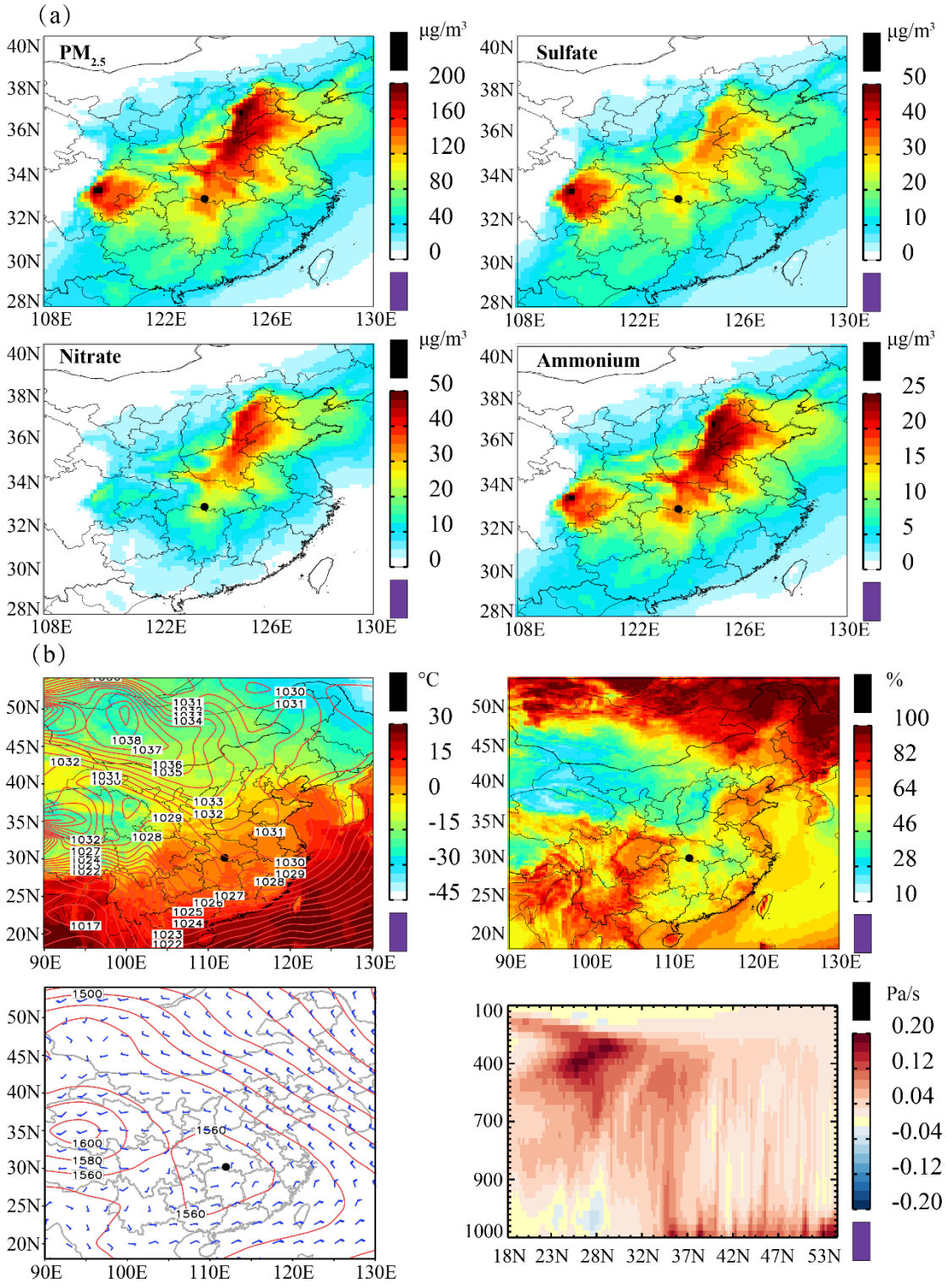

Figure 10 As in Fig. 6 but for A-type synoptic control (14-21 January, 2014).

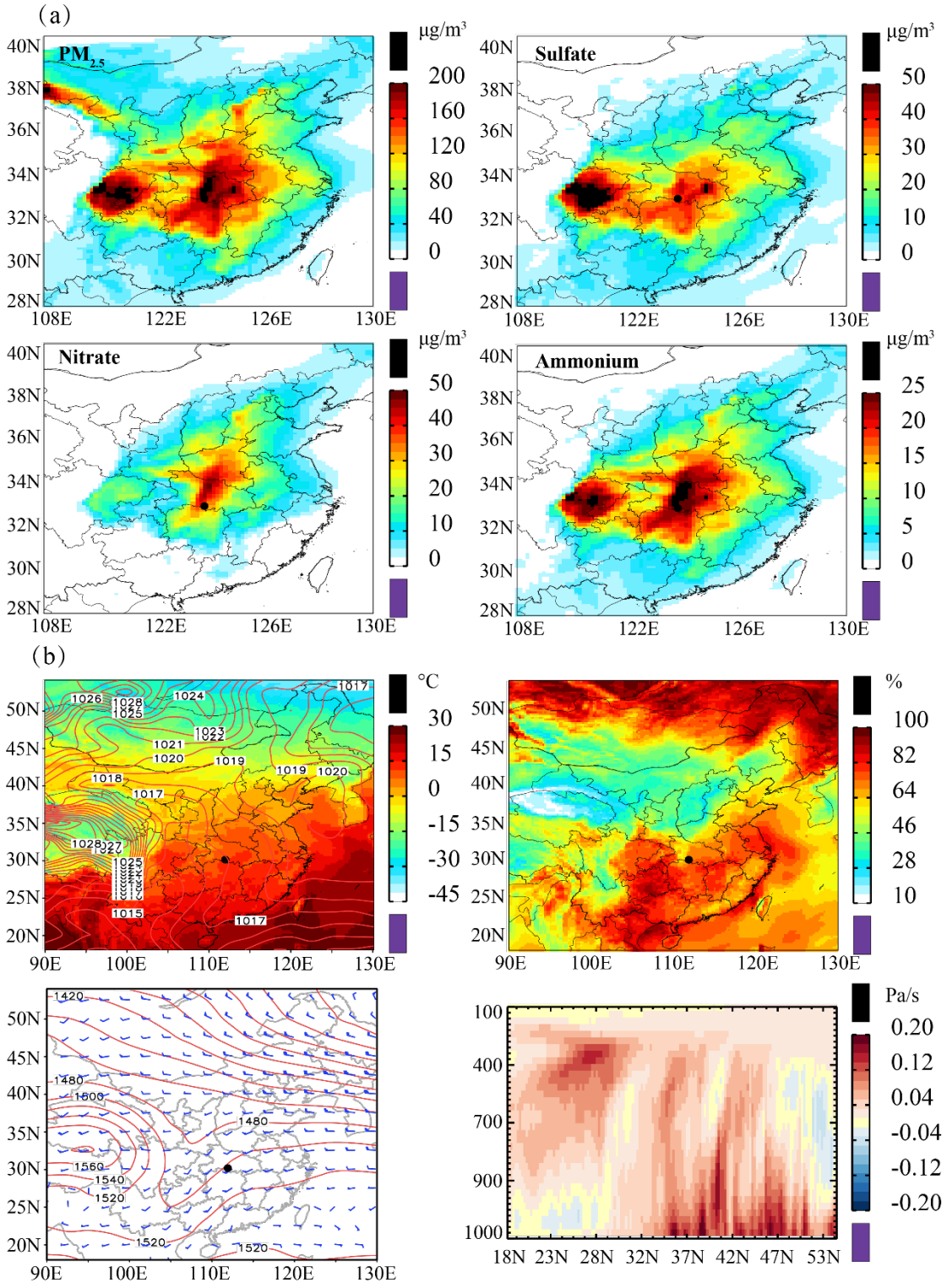

Figure 11 As in Fig. 6 but for C-type synoptic control (26 January - 2 February, 2014).

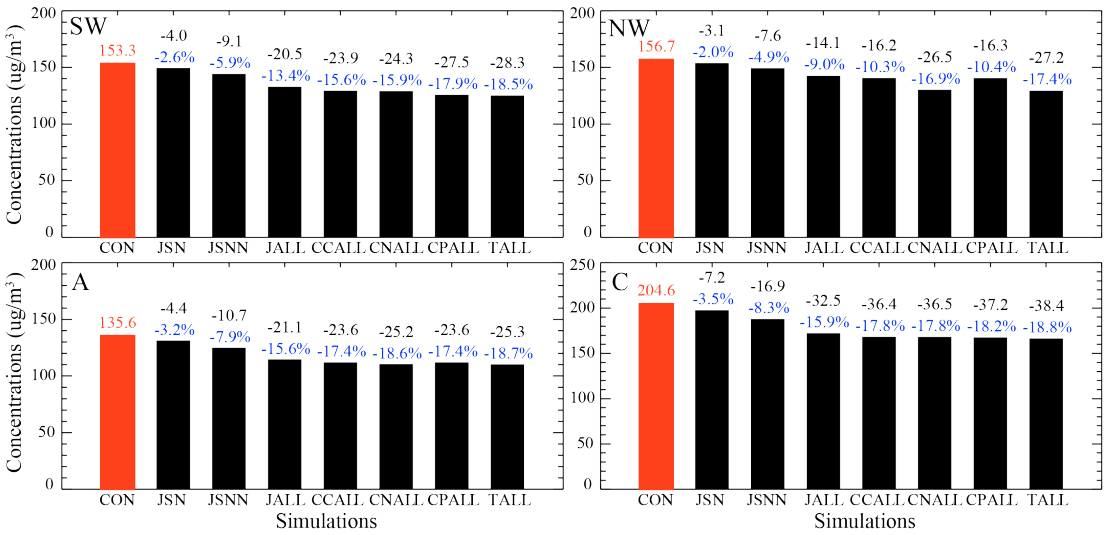

Figure 12 Modeled concentrations (μg/m^3) of $PM_{2.5}$ at Jingzhou in the GEOS-Chem control (red bar) and sensitivity (black bar) simulations for emission reduction, and the differences (black characters for mass concentrations and blue characters for mass percentages) between the sensitivity and the control simulations. The abbreviations of each simulation referred to Table 2.

1013

1014 Table 1 Lamb-Jenkinson circulation types

$\lvert\xi\rvert \leq V$	$\lvert\xi\rvert \geq 2V$	$V < \lvert\xi\rvert < 2V$
(Flat airflow type)	(Rotating airflow type)	(Mixed type)
East (E), Southeast (SE), Southwest (SW), Northwest (NW)	Anticyclone (A), Cyclone (C)	Cyclone-Southeast (CSE), Cyclone-West (CW), Cyclone-Northwest (CNW), Anticyclone-West (AW)

1015

1016

Table 2 Description of sensitivity simulations by GEOS-Chem model. The NCP, YRD, PRD and SCB are the areas framed in red showed by Fig. 1.

Simulations	Description
CON	Applying the original emission situation in Table S1 and Table S2
XJ0	Emissions of all pollution sources[1] outside Jingzhou are set to be zero
XCC0	Emissions of all pollution sources outside Central China are set to be zero
NCP0	Emissions of all pollution sources over NCP region are set to be zero
YRD0	Emissions of all pollution sources over YRD region are set to be zero
PRD0	Emissions of all pollution sources over PRD region are set to be zero
SCB0	Emissions of all pollution sources over SCB region are set to be zero
JSN	Emissions of SO_2 and NO_x at Jingzhou are reduced by 20%
JSNN	Emissions of SO_2, NO_x and NH_3 at Jingzhou are reduced by 20%
JALL	Emissions of all pollution sources at Jingzhou are reduced by 20%
CCALL	Emissions of all pollution sources over Central China are reduced by 20%
CNALL	Emissions of all pollution sources over Central China and NCP region are reduced by 20%
CPALL	Emissions of all pollution sources over Central China and PRD region are reduced by 20%
TALL	Emissions of all pollution sources over Central China, NCP, YRD, PRD and SCB region are reduced by 20%

1. All pollution sources include emissions of SO_2, NO_x, NH_3, CO, BC, OC and NMVOCs.

1024

1025 Table 3 Simulated $PM_{2.5}$ concentrations and associated chemical components averaged
1026 for the four typical heavy pollution episodes at Jingzhou. Also shown in brackets are
1027 the percentages of each component in $PM_{2.5}$.

$PM_{2.5}$ components	Typical heavy pollution episodes			
μg/m^3	11/18-11/25（SW-type）	12/19-12/26（NW-type）	1/14-1/21（A-type）	1/26-2/2（C-type）
Nitrate	30.6 (20.0%)	34.6 (22.1%)	23.4 (17.3%)	42.3 (20.7%)
Sulfate	26.5 (13.4%)	30.7 (19.6%)	27.7 (20.4%)	40.4 (19.7%)
Ammonium	18.8 (12.3%)	21.6 (13.8%)	17.1 (12.6%)	27.1 (13.2%)
Dust	24.4 (15.9%)	22.3 (14.2%)	19.8 (14.6%)	29.2 (14.3%)
BC	10.5 (6.8%)	9.6 (6.1%)	9.5 (7.0%)	13.8 (6.7%)
POA	21.6 (14.1%)	18.9 (12.1%)	18.9 (13.9%)	27.7 (13.5%)
SOA	20.9 (13.6%)	19.0 (12.1%)	19.2 (14.2%)	24.1 (11.8%)
$PM_{2.5}$	153.3	156.7	135.6	204.6

1028

1029

1030 Table 4 The reported concentrations of $PM_{2.5}$ and the three inorganic salts (sulfate,
1031 nitrate and ammonium, $\mu g/m^3$) in other cities.

References	Site	Time	$PM_{2.5}$	Sulfate	Nitrate	Ammonium
Cao et al., 2012	Beijing	01/03	115.6±46.6	20.0±4.2 (17.3%)	13.1±4.5 (11.3%)	9.4±4.1 (8.1%)
Cao et al., 2012	Qingdao	01/03	134.8±43.0	21.1±7.7 (15.7%)	19.3±9.2 (14.3%)	15.3±5.2 (11.4%)
Cao et al., 2012	Tianjin	01/03	203.1±76.2	32.5±15.1 (16.0%)	25.2±10.3 (12.4%)	22.2±9.8 (10.9%)
Cao et al., 2012	Xi'an	01/03	356.3±118.4	53.8±25.6 (15.1%)	29.0±10.0 (8.1%)	29.8±11.5 (8.4%)
Cao et al., 2012	Chongqing	01/03	316.6±101.2	60.9±19.6 (19.2%)	18.1±6.4 (5.7%)	28.8±8.9 (9.1%)
Cao et al., 2012	Hangzhou	01/03	177.3±59.5	33.4±16.7 (18.8%)	25.7±14.8 (14.5%)	19.1±10.7 (10.8%)
Cao et al., 2012	Shanghai	01/03	139.4±50.6	21.6±12.3 (15.5%)	17.5±8.7 (12.6%)	14.5±5.9 (10.4%)
Cao et al., 2012	Wuhan	01/03	172.3±67.0	31.4±15.6 (18.2%)	22.2±10.7 (12.9%)	18.4±10.2 (10.7%)
Zhang et al., 2011	Xi'an	03/06-03/07	194.1	35.6 (18.3%)	16.4 (8.4%)	11.4 (5.9%)
Huang et al., 2012	Xi'an	01/06-02/06	235.8±125.1	44.8±31.3 (19.0%)	20.5±14.2 (8.7%)	14.5±10.8 (6.1%)
Wang et al., 2020	Jinan	10/17	104±54	14.4±9.2 (13.8%)	33.4±23.2 (32.1%)	13.0±8.3 (12.5%)
Wang et al., 2020	Shijiazhuang	10/17	152±109	19.3±19.6 (12.7%)	42.8±41.1 (28.2%)	18.2±17.1 (12.0%)
Wang et al., 2020	Wuhan	12/17	117±33	13.6±3.2	26.6±11.1	13.1±3.8

				(11.6%)	(22.7%)	(11.2%)
Wang et al., 2016a	Zhengzhou	01/11-02/11	297±160	48±36 (16.2%)	31±19 (10.4%)	21±16 (7.1%)
Wang et al., 2016a	Zhengzhou	01/12-02/12	234±125	23±10 (9.8%)	22±9 (9.4%)	16±5 (6.8%)
Wang et al., 2016a	Zhengzhou	01/13-02/13	337±168	56±39 (16.6%)	39±20 (11.6%)	31±18 (9.2%)
Luo et al., 2018	Zibo	12/06-02/07	224.9±85.4	40.1±19.2 (17.9%)	18.1±9.0 (8.1%)	21.7±10.2 (9.7%)
Wang et al., 2016b	Shanghai	12/11, 12/12, 12/13	73.9±57.5	12.2±9.2 (16.5%)	14.6±12.2 (19.8%)	8.2±6.7 (11.1%)
Xu et al., 2019	Beijing	02/17-03/17	180.5	20.1 (11.1%)	45.6 (25.3%)	22.5 (12.5%)
Xu et al., 2019	Beijing	05/17-09/17	186.7	20.2 (10.8%)	32.4 (17.4%)	17.1 (9.2%)
Xu et al., 2019	Beijing	10/17-11/17	167.5	17.9 (10.7%)	44.5 (26.6%)	20.9 (12.5%)
Zheng et al., 2016	Beijing	03/10-05/10	65.2±65.1	11.1±10.1 (17.0%)	11.1±11.0 (17.0%)	6.8±6.7 (10.4%)
Zheng et al., 2016	Beijing	07/09-08/09	88.9±39.1	23.0±13.9 (25.9%)	16.2±11.8 (18.2%)	11.8±6.8 (13.3%)
Zheng et al., 2016	Beijing	12/09-02/10	84.0±66.6	8.1±8.3 (9.1%)	8.0±9.6 (9.0%)	5.9±7.1 (6.6%)
Zheng et al., 2016	Guangzhou	11/10	73.3±16.5	16.6±4.0 (22.6%)	5.7±3.8 (7.8%)	6.2±2.0 (8.5%)
Zheng et al., 2016	Shenzhen	12/09	64.6±24.7	20.6±3.5 (31.9%)	4.9±3.5 (7.6%)	4.6±1.0 (7.1%)
Zheng et al., 2016	Wuxi	04/10-05/10	82.1±27.0	12.8±3.8	9.9±6.3	7.0±2.0

				(15.6%)	(12.1%)	(8.5%)
Zheng et al., 2016	Jinhua	10/11-11/11	81.9±26.2	18.3±6.7 (22.3%)	12.6±7.0 (15.4%)	10.4±4.1 (12.7%)
Liu et al., 2018	Chongqing	2012-2013	73.5±30.5	19.7±9.6 (26.8%)	6.5±6.2 (8.8%)	6.1±2.7 (8.3%)
Liu et al., 2018	Shanghai	2012-2013	68.4±20.3	13.6±6.4 (19.9%)	11.9±5.0 (17.4%)	5.8±2.1 (8.5%)
Liu et al., 2018	Beijing	2012-2013	71.7±36.0	11.9±8.2 (16.6%)	9.3±7.5 (13.0%)	5.3±2.7 (7.4%)

1032